RBMX2: A Pivotal Regulator Linking *Mycobacterium bovis* Infection to Epithelial-Mesenchymal Transition and Lung Cancer Progression

Chao Wang[1,2,8] Yongchong Peng[1,2] Hongxin Yang[3,4] Yanzhu Jiang[1,2] Abdul Karim Khalid[1] Kailun Zhang[1,2] Shengsong Xie[1] Luiz Bermudez[5] Yong Yang[6] Lei Zhang[1,2] Huanchun Chen[1] Aizhen Guo[1,2,7 *] Yingyu Chen[1,2*]

1 The National Key Laboratory of Agricultural Microbiology, College of Veterinary Medicine, Huazhong Agricultural University, Wuhan, China, 430000

2 National Animal Tuberculosis Para-Reference Laboratory (Wuhan) of Ministry of Agriculture and Rural Affairs, Huazhong Agricultural University, Wuhan, China, 430000

3 Oncology Collaborative Innovation Center, Inner Mongolia Medical University, Hohhot, Inner Mongolia, China, 01000

4 Oncology Collaborative Innovation Center, Inner Mongolia Medical University, Hohhot, Inner Mongolia, China, 010000

5 Department of Biomedical Sciences, College of Veterinary Medicine, Oregon State University, Corvallis, OR, United States, 97331

6 Department of Surgical Oncology, People's Hospital of Inner Mongolia Autonomous Region, Hohhot, Inner Mongolia, China, 010000

7 Hubei Hongshan Laboratory, Huazhong Agricultural University, Wuhan, China, 430000

8 Center for Infectious Disease Research, School of Medicine, Westlake University, Hangzhou, Zhejiang, China, 310012

.

Correspondence*: Yingyu Chen, chenyingyu@mail.hzau.edu.cn, +86 15972025761

Aizhen Guo, aizhen@mail.hzau.edu.cn.+86 13100712906

CW, YP and HY carried out the experiment and wrote sections of the manuscript and made equal contribution.

Abstract

Tuberculosis (TB) is a complex disease that arises from the dynamic interplay among the pathogen, host, and environmental factors. In 2022, TB affected approximately 10.6 million people worldwide, resulting in 1.3 million deaths. In regions with a high burden of zoonotic TB, Mycobacterium bovis (M. bovis) accounts for nearly 10% of human TB cases. The immune evasion strategies and latent nature of Mycobacterium tuberculosis (M. tb) pose significant challenges to understanding the host immune response to TB infection. In this study, we identify RNA-binding motif protein X-linked 2 (RBMX2) as a novel host factor that may facilitate *M. bovis* infection. However, the molecular mechanisms and functional roles of RBMX2 during M. bovis infection remain poorly understood.

Our findings show that RBMX2 is significantly upregulated across multiple cell types following infection, including embryonic bovine lung (EBL) cells, bovine macrophage (BoMac) cells, bovine pulmonary alveolar primary cells, and human alveolar epithelial cells (A549). Using a combination of global transcriptomic sequencing, proteomic profiling, cell adhesion assays, ChIP-PCR, and Western blotting, we demonstrate that RBMX2 suppresses cell adhesion and tight junction formation in EBL cells while promoting M. bovis adhesion and invasion through activation of the p65 signaling pathway. Importantly, integrated analyses of transcriptomic, proteomic, and metabolomic data reveal that RBMX2 plays a key role in regulating epithelial-mesenchymal transition (EMT), a cellular process closely associated with cancer progression.

To further explore the potential link between RBMX2 and cancer, we analyzed the TIMER2.0 database and found elevated RBMX2 expression in lung adenocarcinoma (LUAD) and lung squamous cell carcinoma (LUSC) tissues compared to normal lung tissues. These findings were corroborated by immunofluorescence staining. Using an M. bovis-infected BoMac-induced EBL-EMT model, we show that RBMX2 promotes EMT through activation of the p65/MMP-9 pathway following infection. Additionally, we validated the EMT process in human lung epithelial cancer cells (H1299), further supporting the involvement of RBMX2 in this transition.

Collectively, our study identifies RBMX2 as a novel host factor that may enhance M. bovis infection and drive infection-induced EMT. These findings provide new insights into the molecular

mechanisms underlying TB pathogenesis and suggest that RBMX2 could serve as a potential target for the development of TB vaccines and therapeutic strategies against TB-associated lung cancer.

Keywords: *Mycobacterium bovis*, RNA-binding motif protein X-linked 2, embryo bovine lung, bovine macrophage, cell tight junction, epithelial–mesenchymal transition, bovine tuberculosis, cell tight junction

Abbreviations

RBMX2 RNA-binding motif protein X-linked 2; EBL embryo bovine lung cells; BoMac bovine macrophage cells; A549 human pulmonary alveolar epithelial cells; TB tuberculosis; *M. bovis Mycobacterium bovis*; *M. tb Mycobacterium tuberculosis*; BCG *Bacillus* Calmette–Guerin; WOAH World Organisation for Animal Health; hpi hours postinfection; *M. smegmatis Mycobacterium smegmatis*; *E. coli Escherichia coli*; p65 RELA proto-oncogene, NF-kB subunit;MAPK mitogen-activated protein kinase; EMT epithelial–mesenchymal transition; PARP poly ADP-ribose polymerase; ZO-1 tight junction protein 1; CLDN-5 claudin 5; OCLN occludin; MMP-9 matrix metallopeptidase 9; SP-A surfactant protein A; GO Gene Ontology; KEGG Kyoto Encyclopedia of Genes and Genomes; WB Western blot; RT-qPCR real-time quantitative polymerase chain reaction; IF immunofluorescence; ECM extracellular matrix; TCGA the cancer genome atlas

Introduction

Tuberculosis (TB) remains a major global health threat, with approximately 10.6 million new cases and 1.3 million deaths reported worldwide in 2022 [1]. Mycobacterium tuberculosis (M. tb) and its zoonotic variant, Mycobacterium bovis (M. bovis), are responsible for a significant proportion of TB cases, particularly in regions with a high burden of zoonotic diseases, where M. bovis accounts for up to 10% of human TB infections. The immune evasion strategies of M. tb and its variants complicate our understanding of host immune responses and disease progression.

Recent studies have increasingly linked chronic infections, including TB, to cancer development [2, 3]. The persistent inflammatory environment induced by chronic infection can drive cellular transformations, such as epithelial-mesenchymal transition (EMT), which is closely

88 associated with cancer initiation and metastasis [4]. However, the specific molecular mechanisms
89 and host factors involved in this infection-cancer axis remain largely uncharacterized.

90 In this context, RNA-binding motif protein X-linked 2 (RBMX2) has emerged as a potential
91 host factor involved in both TB infection and cancer progression. Our previous studies
92 demonstrated that RBMX2 regulates alternative splicing of APAF-1 introns, thereby modulating
93 apoptosis following M. bovis infection [5]. Furthermore, accumulating evidence suggests that its
94 homolog, RBMX, plays dual and context-dependent roles in tumorigenesis, acting as either an
95 oncogene or a tumor suppressor. For example, RBMX is overexpressed in hepatocellular
96 carcinoma [6] and T-cell lymphomas [7], whereas its expression is reduced in pancreatic ductal
97 adenocarcinoma, indicating a complex and tissue-specific regulatory function [8].

98 Despite these findings, the role of RBMX2 in M. bovis infection and its potential involvement
99 in EMT regulation remain largely unexplored. Based on our preliminary data, we hypothesize that
100 RBMX2 promotes M. bovis adhesion and invasion by modulating host cell properties, and further
101 facilitates EMT through activation of the p65/MMP-9 signaling pathway. This study aims to
102 elucidate the molecular mechanisms by which RBMX2 contributes to M. bovis infection and its
103 potential role in infection-associated EMT, thereby providing novel insights into the intersection
104 of TB and lung cancer. These findings may highlight RBMX2 as a promising therapeutic target for
105 TB and TB-related malignancies.

106

107 **Results**

108 **Elevated expression of RBMX2 in *Mycobacterium bovis*-infected cells and tuberculous**
109 **Lesions**

110 M. bovis was used to infect the EBL cell library, which was constructed using CRISPR/Cas9
111 technology in our laboratory, at a multiplicity of infection (MOI) of 100:1. We evaluated cell
112 survival and performed high-throughput sequencing on the viable cells to identify key host
113 factors potentially involved in anti-M. bovis defense. Notably, RBMX2 knockout cells exhibited
114 significant resistance to infection.

115

116

117 Further analysis using AlphaFold Multimer revealed that amino acid residues 56 – 134 of
118 RBMX2 contain an RNA recognition motif (Supplementary Fig. 1A). Additionally, we identified 611
119 RBM family sequences at the bovine protein exon level and classified them into subfamilies based
120 on motif similarity. RBMX2 was predominantly assigned to subfamily VII, which includes proteins
121 such as EIF3G, RBM14, RBM42, RBMX44, RBM17, PUF60, SART3, and RBM25 (Supplementary Fig.
122 1B). Comparative analysis of amino acid sequences indicated a high degree of conservation of
123 RBMX2 across species (Supplementary Table 1).
124 To further validate RBMX2 expression in EBL cells following infection with M. bovis and M.
125 bovis Bacillus Calmette – Guerin (BCG), RNA samples were collected at 24, 48, and 72 hours
126 post-infection (hpi). Real-time quantitative polymerase chain reaction (RT-qPCR) results showed
127 that RBMX2 expression was significantly upregulated after infection with both M. bovis and M.
128 bovis BCG (Figs. 1A and B). Moreover, increased RBMX2 expression was observed in bovine
129 monocyte-derived macrophages (BoMac cells), bovine alveolar type II primary cells, and human
130 lung epithelial cells (A549 cells) following M. bovis infection (Figs. 1C – E). Furthermore, we used
131 WB to verify the expression levels of RBMX2 protein in EBL cells after M. bovis infection. The results
132 showed that M. bovis infection upregulates the expression of RBMX2 protein in EBL cells.(Fig. 1F).
133
134 ***RBMX2* did not affect cell cycle but inhibited epithelial cell survival during *M. bovis***
135 **infection**
136 In generating *RBMX2* monoclonal knockout (KO) cells, monoclonal cells were selected
137 through limited dilution in 96-well plates. Sanger sequencing was conducted to identify different
138 monoclonal cells with distinct knockout sites (Supplementary Fig. 2A). We validated the effect of
139 RBMX2 knockout on the cell cycle using flow cytometry, and the results indicated that RBMX2
140 does not affect the cell cycle.(Supplementary Fig. 2B).
141 To investigate the potential role of *RBMX2* in resistance to *M. bovis* infection, we assessed
142 the survival rate of EBL cells and H1299 cells at different hours post-infection using CCK-8 assay.
143 The findings revealed an enhanced survival rate in both *RBMX2* knockout monoclonal EBL cells
144 following *M. bovis* infection (Fig. 1G). Furthermore, RBMX2-silenced H1299 cells exhibited a
145 higher survival rate compared to H1299 ShNc cells after *M. bovis* infection (Fig. 1H). Notably,

146 *RBMX2* knockout in EBL cells and silencing in H1299 cells demonstrated significant improvements
147 in cells survival at 96 and 120 hpi compared to Wild Type (WT) EBL cells and H1299 ShNC cells, as
148 evidenced by crystal violet staining (Supplementary Fig. 2C).
149
150 ***RBMX2*-regulated genes associated with cell tight junction and EMT-related pathways**
151 To investigate the role of RBMX2 knockout during M. bovis infection, we selected RBMX2
152 knockout EBL cells and wild-type (WT) EBL cells at 0 hours post-infection (hpi) (2 hpi
153 post-gentamicin, referred to as 0 hpi), 24 hpi, and 48 hpi for RNA-Seq analysis. A total of 16,079
154 genes were identified with a significance threshold of $p < 0.05$ and a log2(fold change) > 2 relative
155 to WT EBL cells. Notably, 42 genes were significantly regulated at all three time points (0, 24, and
156 48 hpi) (Fig. 2A). Of these, 11 genes were significantly upregulated, while 31 were significantly
157 downregulated. A heat map illustrating the expression levels of these genes across all samples is
158 presented, with each row representing a gene and each column representing a sample (Fig. 2A).
159 To further explore the functional implications of these differentially expressed genes (DEGs)
160 in RBMX2 knockout EBL cells during infection, Gene Ontology (GO) and Kyoto Encyclopedia of
161 Genes and Genomes (KEGG) pathway analyses were conducted. The most significantly enriched
162 biological processes included epithelial cell differentiation, cell adhesion, and biological adhesion.
163 The most affected cellular components were the extracellular region, extracellular region part,
164 extracellular space, and plasma membrane part. Molecular functions were primarily associated
165 with activin receptor activity, type I (Fig. 2B). KEGG pathway analysis revealed that these DEGs
166 were involved in several pathways, including ECM－receptor interaction, cGMP-PKG signaling
167 pathway, PI3K-Akt signaling pathway, cytokine-cytokine receptor interaction, and vascular
168 smooth muscle contraction (Fig. 2C).
169 Proteomic analysis of 48 hpi protein samples further validated the phenotypes related to
170 cell tight junctions and epithelial-mesenchymal transition (EMT). GO analysis identified significant
171 enrichment in pathways related to extracellular space, integrin binding, basement membrane,
172 and glucose homeostasis, whereas KEGG analysis highlighted pathways such as cell adhesion
173 molecules, ECM－receptor interaction, and the TGF-beta signaling pathway (Figs. 2D and 2E).
174 We also assessed how varying infection durations influenced RBMX2 knockout EBL cells

175 using GO analysis. At 0 hpi, differentially expressed genes were primarily associated with cell
176 junctions, extracellular regions, and cell junction organization (Supplementary Fig. 3A). At 24 hpi,
177 enriched pathways included basement membrane, cell adhesion, integrin binding, and cell
178 migration (Supplementary Fig. 3B). By 48 hpi, genes were mainly annotated to epithelial cell
179 differentiation and were negatively regulated during epithelial cell proliferation (Supplementary
180 Fig. 3C), suggesting that RBMX2 modulates cellular connectivity throughout the stages of M.
181 bovis infection.

182 KEGG analysis revealed distinct enrichment patterns over time. At 0 hpi, genes were
183 enriched in the MAPK signaling pathway, chemical carcinogen-DNA adducts, and chemical
184 carcinogen – receptor activation (Supplementary Fig. 3D). At 24 hpi, significant enrichment was
185 observed in ECM – receptor interaction, PI3K – Akt signaling pathway, and focal adhesion
186 (Supplementary Fig. 3E). At 48 hpi, enrichment was noted in the TGF-beta signaling pathway,
187 transcriptional misregulation in cancer, microRNAs in cancer, small cell lung cancer, and the p53
188 signaling pathway (Supplementary Fig. 3F).

189 To validate the RNA-seq results, we selected 10 genes at random for RT-qPCR analysis (Fig.
190 2F and Supplementary Fig. 4C). The mRNA levels of these genes were consistent with RNA-seq
191 data. These genes included FRMD4B, MCTP1, HSPB8, ST14, and OMD, which are associated with
192 scaffold proteins, cell adhesion, and epithelial barrier function. Additionally, MCTP1, HSPB8, IL-24,
193 IL-7, GPX2, and NOS3 were linked to apoptosis, inflammation, and oxidative stress.

194

195 ***RBMX2* interferes with the integrity of tight junctions in epithelial cells caused by *M. bovis***

196 Through transcriptome sequencing, we identified 41 genes that underwent transcript
197 changes following *M. bovis* infection. Of these, 22 genes were upregulated, while 19 genes were
198 downregulated (Supplementary Figs. 4A and B). The downregulated genes were primarily
199 associated with tight junction and leukocyte transendothelial migration (Fig. 3A). In contrast, the
200 upregulated genes were mainly linked to immunity-related pathways, including the defense
201 response to viruses and regulation of viral processes (Fig. 3B).

202 Based on these finding,we hypothesized that *RBMX2* could damage the integrity of
203 epithelial cell tight junction. To validate this prediction, we constructed a model of *M.*

204 *bovis*-destroyed tight junctions in EBL cells. EBL cells were infected with *M. bovis* and we
205 subsequently performed RT-qPCR and Western blot (WB) analyses to assess the expression of cell
206 tight junction-related mRNAs (*TJP1*, *OCLN*, *CLDN-5*, and *CLDN-7*) and proteins (ZO-1, OCLN, and
207 CLDN-5). We found that the expression levels of most mRNAs and proteins were significantly
208 reduced following *M. bovis* infection compared to the uninfected coutrol (Figs. 3C and D).

209 Tight junctions are critical intercellular adhesion structures that define the permeability of
210 barrier-forming epithelial cells [9]. The ability of epithelial cells to maintain functional intercellular
211 adhesion is essential for forming a tight epithelial protective barrier [10]. To further investigate the
212 effect of *M. bovis* on epithelial cell adhesion, we conducted a cell adhesion assay, revealing a
213 significant decrease in the intercellular adhesion ratio (Fig. 3E). These results validated that *M.*
214 *bovis* can compromise the tight junction of EBL cells.

215 To explore the impact of *RBMX2* on the epithelial cells barrier, we infected RBMX2 knockout
216 and WT EBL cells with *M. bovis* and assessed the expression of epithelial barrier-related mRNAs
217 (*TJP1*, *OCLN*, and *CLDN-5*) and proteins (ZO-1, OCLN, and CLDN-5) using RT-qPCR and WB. The
218 *RBMX2* knockout EBL cells exhibited a significant upregulation of all three proteins compared to
219 WT EBL cells (Figs. 3F and G). The cell adhesion assay also demonstrated that *RBMX2* knockout
220 EBL cells displayed a heightened adhesion ratio relative to WT EBL cells (Fig. 3H).

221 Tight junctions are essential component of the epithelial barrier and can be compromised by
222 bacteria infections, contributing to inflammation [11, 12]. To investigate whether *RBMX2* mediates
223 intracellular inflammation by regulating the tightness of the epithelial barrier, we measured the
224 mRNA levels of inflammatory factors (IL-1β, TNF, and IL-6) in *RBMX2* knockout EBL cells
225 post-infection. The results showed a decrease in the expression of these inflammatory factors in
226 RBMX2 knockout EBL cells compared to WT EBL cells after *M. bovis* infection (Fig. 3I).

227 In summary, our findings indicate that *RBMX2* affects the integrity of epithelial cell tight
228 junctions, and knocking out *RBMX2* enhances tight junction formation while decreasing the
229 inflammatory response induced by *M. bovis*.

230

231

232

233 ***RBMX2* disrupted the epithelial barrier via activating *p65***

234 The MAPK pathway and NF-kappaB pathway play crucial roles in regulating tight junctions
235 between epithelial cells [13-16]. To further elucidate the regulatory mechanism of *RBMX2* in the
236 epithelial barrier's tight junctions, we found that the MAPK pathway was enriched in our
237 transcriptome sequencing data, and the potential regulatory transcription factor p65 was
238 predicted through the JASPAR database (Supplementary Table 2).

239 We assessed the phosphorylation levels of MAPK pathway proteins and p65 in RBMX2
240 knockout EBL cells, revealing a significant reduction in the phosphorylation of p65 and
241 MAPK/p38/JNK in these cells following M. bovis infection compared to wild-type (WT) EBL cells
242 (Figs. 4A and B).

243 To determine whether RBMX2 specifically regulates MAPK/p38/JNK proteins and p65 to
244 promote disruption of tight junctions and reduce intercellular adhesion, RBMX2 knockout EBL
245 cells were treated with PMA (a p65 activator), Anisomycin (a JNK activator), and ML141 (a p38
246 activator) for 12 h prior to M. bovis infection. The optimal concentrations of these activators
247 were determined using Western blotting (WB) and CCK-8 cell viability assays, resulting in
248 concentrations of 100 nM for PMA, 10 μM for Anisomycin, and 10 μM for ML141, with no
249 significant effects on cell viability (Supplementary Figs. 5A, B, and C). WB results indicated that
250 activation of p65 and the MAPK/p38 pathways suppressed the expression of tight junction
251 proteins, including ZO-1, OCLN, and CLDN-5, following M. bovis infection (Figs. 4C and D).

252 To investigate whether RBMX2 regulates the cell adhesion ratio via p65 and MAPK/p38/JNK
253 pathways, we examined the effects of p65, p38, and JNK activators on cell adhesion in RBMX2
254 knockout EBL cells. Cell adhesion assays demonstrated that treatment with the p65 activator
255 significantly reduced the adhesion ratio compared to treatments with the p38 and JNK activators
256 (Figs. 4E and F).

257 To further confirm the association between p65 and tight junction regulation in WT EBL cells
258 after M. bovis infection, we used siRNA to knock down p65 expression. WB analysis showed that
259 siRNA effectively reduced both p65 and phosphorylated p65 (p-p65) expression (Figs. 4G and H).
260 Furthermore, WB results revealed that p65 suppression enhanced the expression of ZO-1, OCLN,
261 and CLDN-5 following M. bovis infection (Figs. 4G and H). Additionally, silencing p65 in WT EBL

262 cells inhibited M. bovis invasion into epithelial cells, as demonstrated by plate counting assays
263 (Fig. 4I).
264 Finally, to investigate the relationship between *RBMX2*-mediated p65 and the findings above,
265 EBL cells were infected with *M. bovis* and *M. bovis* BCG. WB and high-content live imaging system
266 outcomes demonstrated diminished nuclear translocation of the p65 protein in *RBMX2* knockout
267 EBL cells compared with WT EBL cells (Figs. 4J and K).
268 In summary, our findings validate that *RBMX2* can regulate the phosphorylation and nuclear
269 translocation of p65 protein, leading to the degradation of tight junction proteins in EBL cells
270 infected with *M. bovis*.
271
272 ***RBMX2* promotes adhesion, invasion, and intracellular survival of pathogens**
273 Disrupting the intercellular tight junction barrier enhances bacterial adhesion and invasion [17,
274 18]. Based on these findings, we hypothesize that *RBMX2* may facilitate the adhesion and invasion
275 of *M. bovis* by degrading the tight junction proteins in EBL cells. To test this hypothesis, EBL cells
276 were infected with *M. bovis* at an MOI of 20:1, plate count assays indicated a significant
277 reduction in *M. bovis* adhesion in *RBMX2*-KO#17 and KO#23 EBL cells compared with WT EBL cells
278 at 15 min, 30 min, 1 h, and 2 h post-infection (Supplementary Fig. 6A) . Furthermore, the invasion
279 of *M. bovis* in *RBMX2*-KO#17 and KO#23 EBL cells were decreased at 2, 4, and 6 h post-infection
280 compared with WT EBL cells (Supplementary Fig. 6B). Additionally, the intracellular survival of *M.*
281 *bovis* in *RBMX2*-KO#17 and KO#23 EBL cells was lower at 24, 48, 72 and 96 hpi compared with
282 WT EBL cells (Supplementary Fig. 6C). Silencing *RBMX2* in human lung epithelial cells (H1299)
283 also led to a significant reduction in the adhesion, invasion, and intracellular survival of *M. bovis*
284 (Supplementary Figs. 6D-F). Thus, the host factor *RBMX2* is critical for promoting the adhesion,
285 invasion, and intracellular survival of *M. bovis*. In addtion, pathway activators were employed to
286 investigate the relationship between pathway activation and the regulation of *M. bovis* adhesion
287 and invasion by *RBMX2*. The results showed that applying a p65 activator to *RBMX2* knockout EBL
288 cells significantly impaired the tight junction function of the epithelial barrier, thereby enhancing
289 *M. bovis* adhesion and invasion in EBL cells by regulating the phosphorylation and nucleation of
290 p65 (Supplementary Figs. 7A and B). Hence, RBMX2 promotes *M. bovis* adhesion and invasion in

291 EBL cells by regulating the phosphorylation and nucleation of p65.

292 To further investigate the role of RBMX2 in adhesion and invasion across different virulent
293 mycobacterial species, we employed both attenuated virulent Mycobacterium bovis BCG and
294 Mycobacterium smegmatis (M. smegmatis) to infect EBL cells. Plate count assays demonstrated a
295 significant decrease in the adhesion of both M. bovis BCG and M. smegmatis in RBMX2
296 knockout EBL cells at multiple time points post-infection compared to wild-type (WT) EBL cells
297 (Supplementary Figs. 7C and D). Moreover, the invasion of both mycobacterial species was
298 notably reduced at various hours post-infection in RBMX2 knockout cells (Supplementary Figs. 7E
299 and F). These findings suggest that the virulence of Mycobacterium does not influence the ability
300 of RBMX2 to facilitate adhesion and invasion in EBL cells.

301 Additionally, to assess whether RBMX2 regulates interactions with other pathogens
302 associated with bovine pneumonia, EBL cells were infected with Salmonella and Escherichia coli
303 (E. coli). Our results revealed that RBMX2 knockout EBL cells exhibited a reduction in bacterial
304 adhesion and invasion across all tested species compared to WT cells (Supplementary Figs. 7G –
305 J).

306 Collectively, these experiments provide strong evidence that RBMX2 broadly enhances the
307 adhesion and invasion of pathogens linked to bovine pneumonia, underscoring its potential as a
308 therapeutic target for developing disease-resistant cattle.

309 ***RBMX2* is highly expressed in lung cancer and regulates cancer-related metabolites**

310 Previous studies have demonstrated a link between bacterial infection and the initiation of
311 EMT [19-21]. Prolonged infection with *M. tb* or *M. bovis* induces oxidative stress, activates Toll-like
312 receptors (TLR), and elicits the release of inflammatory cytokines [22-24]. Consequently, this
313 phenomenon creates a favorable microenvironment for tumor development, progression, and
314 dissemination [25, 26]. Epidemiological investigations have established a correlation between TB and
315 the occurrence of lung cancer [27-30]. However, the precise cellular mechanism underlying this
316 association remain unclear.

317 In our research, we conducted a comprehensive analysis of gene families, revealing a
318 remarkable degree of *RBMX2* conservation among bovine, monkey, and human sources (Fig. 5A).
319 To further elucidate the involvement of *RBMX2* in cancer, we utilized the *TIMER2.0* database to

320 assess its expression patterns across various cancer types within The Cancer Genome Atlas
321 (TCGA). Our findings indicated a notable upregulation of *RBMX2* in lung cancer, specifically in
322 lung adenocarcinoma (LUAD) and lung squamous cell carcinoma (LUSC) (Fig. 5B).

323 To investigate the elevated expression of *RBMX2* in lung cancer further, we measured its
324 expression in both lung cancer epithelial cell lines and normal lung epithelial cell lines using
325 RT-qPCR. The results demonstrated that *RBMX2* expression in lung cancer epithelial cell lines
326 (NCIH1299, NCIH460, and CALU1) was significantly higher than that in normal lung epithelial cells
327 (BEAS-2B) (Fig. 5C). Additionally, immunofluorescence (IF) analysis revealed that *RBMX2*
328 expression levels were also higher in LUAD and LUSC tumor tissues compared to adjacent
329 non-cancerous lung tissues (Figs. 5D-F).

330 Furthermore, we investigate whether *RBMX2* regulates specific EMT-related metabolites to
331 mediate the EMT process in EBL cells following *M. bovis* infection. Our metabolomic analysis of
332 EBL cell samples at 48 hpi revealed that *RBMX2* knockout primarily enriched pathways related to
333 nucleotide metabolism, biosynthesis of cofactors, biosynthesis of nucleotide sugars, pentose and
334 glucuronate interconversions, vascular smooth muscle contraction, amino sugar, and nucleotide
335 sugar metabolism, chemokine signaling pathway, aldosterone synthesis and secretion, and
336 cGMP-PKG signaling pathway. Thes pathways are associated with tumor cells proliferation,
337 migration, and invasion (Fig. 5G). Differential metabolites are related to tumor metabolism,
338 mainly including 6-glucuronic acid estriol, adenosine, uridine 5 '- triphosphate, and 5' - deoxy-5 '-
339 (methylthio) (Figure 5H).

340

341 ***RBMX2* promotes the transformation of EBL cells from epithelial cells to mesenchymal**
342 **cells**

343 To investigate the association between *RBMX2* and EMT induced by *M. bovis*, we intially
344 infected EBL cells directly with *M. bovis*. This infection did not effectively induce the expression of
345 mesenchymal cell marker proteins (Supplementary Fig. 8A). Previous literature indicates that *M.*
346 *bovis* infection in macrophages, along with its secreted proteins, can stimulate the production of
347 cytokines such as TNF, IL-6, and TGF-β, all of which promote EMT process [31-34].

348 To further explore the impact of *M. bovis* infection on EMT progression in EBL cells, we

349 constructed a coculture model using *M. bovis*-infected BoMac cells (Fig. 6A and Supplementary
350 Fig. 8B). In this model, we identified EMT-related cytokines, including IL-6 and TNF, in *M.*
351 *bovis*-infected BoMac cells, revealing a significant increase compared to uninfected BoMac and
352 EBL cells (Fig. 6B). Notably, *RBMX2* expression was upregulated in EBL cells within this coculture
353 model following *M. bovis* infection (Fig. 6C).

354 We then examined the morphology changes in epithelial cells within the coculture model
355 using electron microscopy. The results demonstrated that most cells transitioned from circular to
356 an elongated morphology (Fig. 6D). Staining of the EBL cells cytoskeleton with ghost pen cyclic
357 peptide highlighted significant morphological alterations, with EBL cells transforming from
358 spherical to spindle-shaped (Supplementary Fig. 8C).

359 Additionally, we assessed the expression of EMT-related mRNAs and proteins in EBL cells
360 after coculture with *M. bovis-infected* BoMac cells. This analysis reveald a significant
361 downregulation of the epithelial cell marker protein *E-cadherin* and a notable upregulation of
362 mesenchymal markers *N-cadherin* and *MMP-9*, as determined by RT-qPCR and WB (Fig. 6E,
363 Supplementary Fig. 8D). The coculture with, *M. bovis-infected* BoMac cells enhanced the
364 migratory and invasive properties of EBL cells, as demonstrated by Transwell assay (Figs. 6F and
365 G).

366 To confirm the impact of *RBMX2* knockout on the EMT process in the coculture model, we
367 observed that *RBMX2* knockout cells exhibited significant upregulation of the epithelial cell
368 marker protein *E-cadherin* and downregulation of the mesenchymal cell marker *N-cadherin* and
369 *MMP-9* compared to WT EBL cells, as shown by RT-qPCR and WB (Fig. 6H and Supplementary Fig.
370 7E). Wound healing and Transwell assays demonstrated that the migration and invasion rates of
371 *RBMX2* knockout cells were markedly lower than those of WT EBL cells (Figs. 6I, J, and K).

372 Finally, we silenced RBMX2 in the human lung cancer epithelial cell line H1299, which
373 expresses high levels of RBMX2, to assess the effect on EMT-related proteins, as well as invasion
374 and migration ability following *M. bovis* infection. The results indicated that RBMX2 significantly
375 inhibited the EMT process in H1299 cells post-infection (Supplementary Figs. 9A and B).

376 In conclusion, we successfully established a coculture model involving *M. bovis*-infected
377 BoMac cells that induce EMT in EBL cells, thereby demonstrating that the host factor *RBMX2*

effectively promotes the EMT process in this context.

***RBMX2* facilitates the EMT process via the *p65/MMP-9* pathway**

EMT enhances the migration and invasion capabilities of tumor cells [35-37]. Both p65 and *MAPK/p38/JNK* pathways have been shown to regulate the EMT process through various mechanisms. [38-41]. To elucidate the precise regulatory role of *RBMX2* in the EMT process within the coculture model of EBL cells, we assessed the *MAPK* pathway and p65 protein levels via WB. Our findings revealed a significant reduction in the phosphorylation of *p65* and *MAPK/p38/JNK* in *RBMX2* knockout cells infected with *M. bovis,* compared to WT EBL cells (Supplementary Fig. 9C).

To identify the specific signaling pathways regulating the EMT phenotype involving p65 and MAPK/p38/JNK in the coculture model, RBMX2 knockout EBL cells were treated with PMA, Anisomycin, and ML141. Our results showed that p65 suppresses E-cadherin expression while enhancing MMP-9 expression (Fig. 7A). Activation of the MAPK/p38 pathway inhibits E-cadherin expression and promotes N-cadherin expression. In contrast, the MAPK/JNK pathway suppresses N-cadherin expression while enhancing the expression of both E-cadherin and MMP-9. Furthermore, a comprehensive analysis of the relationship between pathway activation and cellular migration and invasion revealed that activation of the p65 pathway increases the migratory and invasive abilities of EBL cells, as demonstrated by Transwell assays (Figs. 7B and C) and wound-healing assays (Figs. 7D and E).

Invasion and migration are critical stages in tumor development, influenced by *p65*-dependent factors such as matrix metalloproteinases, urokinase fibrinogen activators, and interleukin-8 [42-46]. To further substantiate the correlation between the p65 protein and the regulation of the EMT process in EBL cells post-*M. bovis* infection, we employed siRNA to inhibit p65 expression in WT EBL cells. This suppression was found to inhibit *MMP-9* expression, as demonstrated by WB (Figs. 7F and G).

To thoroughly verify the regulatory mechanism between RBMX2 and p65, we initiated our investigation by conducting an in-depth analysis of the RBMX2 promoter region to identify potential interactions with the transcription factor p65. Initially, we performed molecular docking simulations to predict the binding affinity and interaction patterns between RBMX2 and p65

407 proteins. These simulations revealed multiple amino acid residues within the RBMX2 protein that
408 formed strong, stable interactions with p65. The docking analysis yielded a high docking score of
409 1978.643 (Fig. 7K), indicating a significant likelihood of a direct physical interaction between
410 these two proteins.

411 To complement the protein-protein interaction analysis, we next investigated whether p65
412 could directly bind to the promoter region of the RBMX2 gene at the transcriptional level. Using
413 the JASPAR database, a comprehensive resource for transcription factor binding profiles, we
414 queried the RBMX2 promoter sequence for potential p65 binding sites. This analysis identified
415 several putative binding motifs, suggesting that p65 may act as a transcriptional regulator of
416 RBMX2 expression.

417 To experimentally validate this transcriptional regulatory relationship, we employed a
418 dual-luciferase reporter assay. We cloned the RBMX2 promoter region containing the predicted
419 p65 binding sites into a luciferase reporter plasmid. This construct was then co-transfected into
420 cultured cells along with a plasmid expressing p65. The luciferase activity was significantly
421 increased in cells expressing p65 compared to control groups, providing functional evidence that
422 p65 enhances the transcriptional activity of the RBMX2 promoter (Fig. 7I).

423 Furthermore, to confirm the direct binding of p65 to the RBMX2 promoter in a chromatin
424 context, we performed chromatin immunoprecipitation followed by quantitative PCR (ChIP-qPCR).
425 In this assay, we used specific antibodies against p65 to immunoprecipitate chromatin fragments
426 containing p65-bound DNA. The enriched DNA fragments were then analyzed using primers
427 targeting the RBMX2 promoter region. Our results demonstrated a significant enrichment of the
428 RBMX2 promoter in the p65 immunoprecipitated samples compared to the IgG control, thereby
429 confirming that p65 physically associates with the RBMX2 promoter in vivo (Fig. 7J). Collectively,
430 these findings-ranging from computational docking predictions to transcriptional reporter assays
431 and ChIP validation-provide strong evidence supporting a direct regulatory interaction between
432 p65 and RBMX2. This regulatory mechanism may play a critical role in the biological pathways
433 involving these two molecules, particularly in contexts such as inflammation, immune response,
434 or cellular stress, where p65 (a subunit of NF-κB) is known to be prominently involved.

435 Moreover, MMP-9 is known to induce EMT in epithelial cells, enhancing their invasiveness.

436 The regulatory mechanisms involving p65 and *MMP-9* have been documented in several studies
437 [47, 48]. In our research, we identified multiple binding sites in the promoter sequences of p65 and
438 MMP-9 through molecular docking (Fig. 7L) and confirmed the biding site between *MMP-9*
439 promoter and *p65* protein via Chip-PCR (Fig. 7M). Using protein docking, we validated the
440 relationship between bovine p65 protein and MMP-9, with a binding score of 1784.378 (Fig. 7N).
441 In summary, *RBMX2* facilitates the EMT process of EBL cells following *M. bovis* infection by
442 activating the *p65/MMP-9* pathway.
443
444 **Discussion**
445 The resurgence of *M. bovis*-associated TB presents a substantial global challenge, affecting
446 both livestock and human populations. Notably, *M. bovis* exhibits over 99% nucleotide similarity
447 with *M. tb* [49]. The pathogenesis of TB is complex process influenced by a confluence of bacterial,
448 host, and environmental factors. Both *M. tb* and *M. bovis* have evolved sophisticated strategies to
449 evade host immune responses, enabling their long-term intracellular persistence. It is estimated
450 that approximately one-third of the global population harbors latent TB infections [50, 51].
451 The successful establishment of infection by mycobacteria is contingent upon their ability to
452 circumvent early innate immune defenses, employing both transcriptional and
453 post-transcriptional regulatory strategies within host macrophages [52-56]. Despite notable
454 advancements in the field, unraveling the mechanisms of immune evasion and understanding the
455 dynamics of latent infections caused by *M. tb* and *M. bovis* remains a substantial challenge. The
456 cellular immune response to these pathogens is inherently complex, further compounded by the
457 microdiversity of mycobacteria within individual hosts and the variability of immune responses
458 among different individuals [54, 57].
459 Lung epithelial cells serve as the primary physical barrier against infection and play a pivotal
460 role in the innate immune response. These cells not only function as a frontline defense but also
461 recruit and activate antigen-presenting cells, such as macrophages, to initiate adaptive immune
462 responses against *M. bovis* infection [58, 59]. Given that alveolar epithelial cells can act as reservoirs
463 for *M. bovis*, their role in the infection process is particularly significant. Additionally, activated
464 macrophages and neutrophils enhance the bactericidal effects of alveolar epithelial cells, further

465 contributing to the host's defense mechanisms [60, 61].

466 In our study, we employed a CRISPR-Cas9 mutant library generated in our laboratory to
467 explore potential host factors involved in M. bovis infection. Notably, we identified RBMX2 as a
468 protein that significantly promotes M. bovis infection. The *RBMX2* protein, characterized by an
469 RNA recognition motif within its 56-134 amino acid residue region, is implicated in mRNA splicing
470 through spliceosomes and is emerging as a potential molecular marker for sperm activity. [62]. The
471 downregulation of RBMX2 in the X chromosome of lung telocytes suggests its involvement in
472 cellular immunity [63].

473 Further exploration of RBM genes in cattle revealed that EIF3G, RBM14, RBM42, RBMX44,
474 RBM17, PUF60, SART3, and RBM25 belong to the same subfamily as RBMX2. Previous studies
475 have demonstrated that genes within this subfamily can regulate the proliferation and lifecycle of
476 cancer cells. For instance, EIF3G modulates the mTOR signaling pathway, inhibiting the
477 proliferation and metastasis of bladder cancer cells [64]. Similarly, RBM14 has been linked to the
478 reprogramming of glycolysis in lung cancer, acting as a novel epigenetically activated oncogene [60].
479 Despite these insights, the specific function of RBMX2 in the context of *M. bovis* infection and its
480 potential role in cancer pathogenesis remain largely unexplored.

481 Our findings reveal that *RBMX2* is upregulated in TB-infected cells, demonstrating its
482 capacity to enhance *M. bovis* infection. Transcriptomic analyses suggest that *RBMX2* may disrupt
483 tight junctions within epithelial cells and promote EMT following *M. bovi*s infection.

484 Epithelial cells serve as more than passive barriers; they actively participate in innate
485 immunity by regulating cytokine secretion and maintaining barrier integrity [61]. Disruptions in
486 epithelial tight junctions, often exacerbated by pro-inflammatory stimuli from pathogenic
487 bacteria, can facilitate bacterial translocation and subsequent infection [61 65, 66]

488 In our experiments, we observed that the disruption of the epithelial barrier facilitated *M.*
489 *bovis* adhesion and invasion. Conversely, the knockout of RBMX2 stabilized the epithelial barrier,
490 attenuating *M. bovis* invasion and intracellular survival. This stabilization also mitigated
491 downstream innate immune responses, reducing cellular inflammation, ROS production, and
492 apoptosis.

493 The loss of tight junction integrity is a precursor to EMT, a process increasingly recognized

494 for its role in cancer progression [20, 65-67]. Recent studies have established a link between bacterial
495 infections and EMT induction, particularly in the context of gastric adenocarcinomas [68, 69].
496 Epidemiological evidence suggests that TB may serve as a risk factor for lung cancer [70, 71];
497 however, the underlying cellular mechanisms remain elusive. Chronic TB infection has been
498 implicated in lung carcinogenesis, with reports indicating that BCG vaccination can enhance the
499 survival of tumor cells under inflammatory conditions [72 73]. There is growing epidemiological
500 evidence suggesting that chronic TB infection represents a potential risk factor for the
501 development of lung cancer. Studies have shown that individuals with a history of TB exhibit a
502 significantly increased risk of lung cancer, particularly in areas of the lung with pre-existing
503 fibrotic scars, indicating that chronic inflammation, tissue repair, and immune microenvironment
504 remodeling may collectively contribute to malignant transformation [74]. Moreover, EMT not only
505 endows epithelial cells with mesenchymal features that enhance migratory and invasive capacity
506 but is also associated with the acquisition of cancer stem cell-like properties and therapeutic
507 resistance [75]. Therefore, EMT may serve as a crucial molecular link connecting chronic TB
508 infection with the malignant transformation of lung epithelial cells, warranting further
509 investigation in the intersection of infection and tumorigenesis.

510 Moreover, *M. tb*-infected THP-1 cells have been shown to induce EMT in lung
511 adenocarcinoma epithelial cells [76]. Chronic infection with *M. tb* is associated with oxidative stress
512 and inflammatory cytokine production, fostering an environment conducive to tumor progression
513 [77, 78]. Our analysis of RBMX2 across various cancers revealed increased expression levels in lung
514 adenocarcinoma (LUAD) and lung squamous cell carcinoma (LUSC), suggesting a conserved role in
515 tumor biology across species.

516 In light of these findings, we constructed a model of *M. bovis* infection in EBL cells to
517 investigate EMT induction. Initial results indicated that *M. bovis* alone did not induce EMT;
518 however, a co-culture model incorporating *M. bovis*-infected BoMac cells successfully induced
519 EMT in EBL cells. Notably, the knockout of RBMX2 in this context inhibited EMT, suggesting that
520 RBMX2 may elevate the risk of lung cancer through EMT induction following *M. bovis* infection.
521 Meanwhile, metabolic pathways enriched after RBMX2 knockout, such as nucleotide metabolism,
522 nucleotide sugar synthesis, and pentose interconversion, primarily support cell proliferation and

migration during EMT by providing energy precursors, regulating glycosylation modifications, and maintaining redox balance; cofactor synthesis and amino sugar metabolism participate in EMT regulation through influencing metabolic remodeling and extracellular matrix interactions; chemokine and cGMP-PKG signaling pathways may further mediate inflammatory responses and cytoskeletal rearrangements, collectively promoting the EMT process.

In summary, RBMX2 drives TB pathogenesis by compromising epithelial barriers and inducing EMT. Targeting RBMX2 may present a promising avenue for the prevention and treatment of TB in both humans and animals. Additionally, the effective modulation of *RBMX2* could potentially mitigate the incidence of TB-associated EMT and its implications for lung cancer development in the near future.

Conclusion

Our research findings indicate that RBMX2 significantly enhances the invasive capacity of Mycobacterium bovis by promoting the activation and nuclear translocation of the p65 protein. This activation compromises the integrity of the epithelial cell barrier and induces epithelial-mesenchymal transition (EMT) through the p65/MMP-9 signaling pathway. These results highlight the crucial role of RBMX2 in M. bovis pathogenesis and underscore its potential as a therapeutic target for preventing infection-related complications.

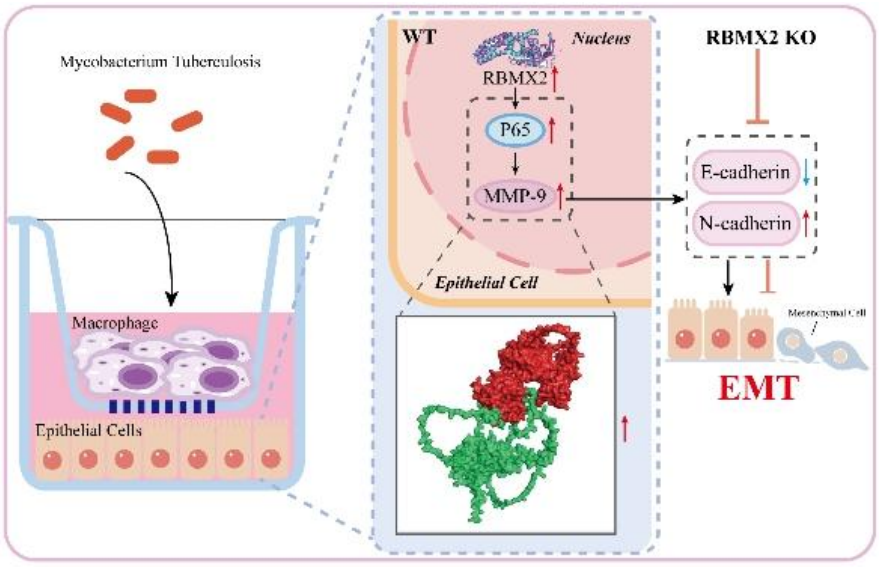

544 **Methods**

545 Patients and lung tissues

546 This study was approved by the Ethics Committee of Inner Mongolia Autonomous Region
547 People's Hospital, and written informed consent was obtained from all participating patients
548 (Approval Number: No. 2020021). A total of 35 specimens of lung cancer tissue, along with
549 adjacent normal lung tissue, were collected. We randomly selected the above specimens,
550 including age and gender. All patients involved in this study had not received any medication,
551 chemotherapy, or radiation therapy prior to surgical resection. The samples were subsequently
552 prepared for immunohistochemistry (IHC) and fluorescence in situ hybridization (FISH) assays.

553 Bovine clinical tissues

554 This project has received approval from the Experimental Animal Ethics Center of Huazhong
555 Agricultural University (Approval Number: HZAUCA-2024-0014). Following examination by
556 researchers at the National Animal Tuberculosis Professional Laboratory (Wuhan), bovine
557 tuberculosis tissue samples were collected from the lungs and livers of slaughtered cattle, with
558 each specimen measuring at least 5 cm × 5 cm × 5 cm and specifically including tissues exhibiting
559 tuberculous lesions.

560

561 Cell lines

562 EBL and 293T RRID:CVCL_0063 cells were generously provided by M. Heller from
563 Friedrich-Loeffler-Institute. These cells were cultured in heat-inactivated 10% fetal bovine serum
564 supplemented with Dulbecco's modified Eagle medium (DMEM, Gibco, USA) at 37°C and 5% CO_2
565 [79]. BoMac cells were kindly provided by Judith R. Stabel from the Johne's Disease Research
566 Project at the United States Department of Agriculture in Ames, Iowa, and were maintained
567 according to previously established protocols [80]. BoMac cells were grown in heat-inactivated 10%
568 fetal bovine serum supplemented with Roswell Park Memorial Institute 1640 (RPMI 1640, Gibco,
569 USA) at 37°C and 5% CO_2. Bovine lung alveolar primary cells were isolated in our laboratory and
570 cultured in heat-inactivated 10% fetal bovine serum supplemented with DMEM (Gibco, USA) at
571 37°C and 5% CO_2. BEAS-2B RRID:CVCL_0168, NCIH1299, NCIH460 RRID:CVCL_0459, and CALU1
572 epithelial cells were all provided by Professor Shi Lei from Lanzhou University, and all culture

573 procedures were conducted according to standardized protocols. We conduct regular testing on
574 all cell lines to eliminate contamination from mycoplasma and black fungus.
575
576 Bacterium
577 *M. bovis* (ATCC:19210), originally isolated from a cow, is maintained in this laboratory. *M.*
578 *smegmatis* mc^2155 (NC_008596.1) and *M. bovis* BCG-Pasteur (ATCC:35734) were generously
579 provided by Professor Luiz Bermudez from Oregon State University. All strains were cultured in a
580 Middlebrook 7H9 broth (BD, MD, USA) supplemented with 0.5% glycerol (Sigma, MO, USA), 10%
581 oleic acid–albumin–dextrose–catalase (OADC, BD, USA) and 0.05% Tween 80 (Sigma, MO, USA) or
582 on Middlebrook 7H11 agar plates (BD, MD, USA) containing 0.5% glycerol (Sigma, MO, USA) and
583 10% OADC (BD).
584 Prior to infection, the optical densities of bacterial cultures at 600 nm (OD600) were
585 adjusted to the required MOI using the standard turbidimetric card. The cultures were then
586 centrifuged at 3,000 g for 10 min. The precipitated bacteria were resuspended in medium and
587 dispersed using an insulin syringe. Subsequently, 50 μL of 10-fold serially diluted bacterial
588 suspension was plated onto Middlebrook 7H11 agar to determine the number of viable bacteria
589 (colony-forming units, CFUs). All experiments involving *M. bovis* were conducted in strict
590 accordance with the biosafety protocols established for the Animal Biosafety Level 3 Laboratory
591 of the National Key Laboratory of Agricultural Microbiology at Huazhong Agricultural University.
592 *E. coli* (ATCC:25922) was donated by Professors Zhou Rui and Wang Xiangru of Huazhong
593 Agricultural University, while *Salmonella* (ATCC:14028) has been preserved and passed down
594 through generations in our laboratory. These strains were resuscitated, and single colonies were
595 purified, cultured, and grown in Luria–Bertani broth.
596
597 Generation of the *RBMX2*-KO EBL cells
598 The small guide RNA (sgRNA) sequence targeting the bovine RBMX2 gene (5'
599 -GAATGAGCGTGAGGTCGAAC-3') was cloned into the lentiviral vector
600 pKLV2-U6gRNA5(BbsI)-PGKpuro2ABFP (#67991), kindly provided by Professor Zhao Shuhong from
601 Huazhong Agricultural University, to generate the recombinant lentivirus. EBL cells were infected

602 with either the RBMX2-targeting lentivirus or the empty vector lentivirus as a negative control. At
603 48 to 60 hours post-infection (hpi), puromycin (2.0 mg/mL) was added to select for stably
604 transduced cells. Positive clones were subsequently enriched and monoclonal cell lines were
605 obtained through limiting dilution. Successful knockout of RBMX2 was confirmed by PCR
606 analysis..Table S1

sgRNA	sequence
sgRNA- F	5′-CCTTGCCCAATTTTTCGGAGG-3′
sgRNA- R	5′-ACAGGAGGATGGTAGTAACGG-3′

607

608

609 Extraction of total RNA and RT-qPCR

610 Cold phosphate-buffered saline (PBS, HyClone, China) was used to wash the cells three times,
611 after which 1 mL of Trizol (Invitrogen, USA) was added per well to lyse the cells. The lysate was
612 collected in EP tubes, and 200 µL of chloroform was subsequently added. The mixture was
613 vortexed for 30 seconds and then centrifuged at 12,000 rpm for 10 minutes at 4°C. Following
614 centrifugation, 500 µL of the supernatant was transferred to a new EP tube. To this supernatant,
615 500 µL of isopropanol was added and mixed gently by inversion. The mixture was allowed to
616 stand for 10 minutes at 4°C before being centrifuged again at 12,000 rpm for 15 minutes at 4°C.
617 The supernatant was discarded, revealing the RNA pellet. Next, the RNA pellet was washed with
618 1 mL of 75% ethanol and centrifuged at 7,500 rpm for 5 minutes at 4°C. The supernatant was
619 removed, and the RNA pellet was air-dried for 15 minutes. Subsequently, 20 µL of DEPC-treated
620 water was added, and the mixture was incubated at 58°C in a water bath for 10 minutes to
621 dissolve the RNA. Purified RNA was then obtained.

622 To assess RNA purity, the OD260/OD280 ratio was measured using a NanoDrop ND-1000
623 instrument (Agilent Inc., USA), with values between 1.8 and 2.0 indicating acceptable purity. RNA
624 integrity and potential contamination with genomic DNA were evaluated using denaturing
625 agarose gel electrophoresis. The samples were stored at -80°C for later analysis.

626 Reverse transcription of the RNA samples was performed using HiScript III RT SuperMix for
627 qPCR (+gDNA wiper, Vazyme, China). Four microliters of 4× gDNA wiper mix were added to 1 µg

628 of RNA, followed by the addition of 16 μL of RNase-free ddH2O. The mixture was incubated at
629 42°C for 2 minutes to eliminate genomic DNA. Reverse transcription was subsequently carried
630 out by adding 4 μL of 5× HiScript III qRT SuperMix, with the mixture incubated at 37°C for 15
631 minutes and then at 85°C for 5 seconds to synthesize cDNA.

632 cDNA expression across different sample groups was quantified using AceQ qPCR SYBR
633 Green Master Mix (Vazyme, China) in a ViiA7 real-time PCR machine (Applied Biosystems Inc.,
634 USA). The final volume of each real-time PCR reaction was 20 μL, comprising 10 μL of 2× AceQ
635 qPCR SYBR Green Master Mix, 0.4 μL of upstream primer (10 μM), 0.4 μL of downstream primer
636 (10 μM), 0.4 μL of 50× ROX reference dye 2, 3 μL of cDNA template, and 5.8 μL of ddH_2O. The PCR
637 conditions were as follows: 95°C for 5 minutes (1 cycle), 95°C for 10 seconds (40 cycles), and 60°C
638 for 30 seconds (40 cycles). The primer sequences for RT-qPCR are provided in Table S2.

639 Table S2

Number	Primer	Sequence
1	Bovine-β-actin-F	5′-AGCAAGCAGGAGTACGATGAG-3′
2	Bovine-β-actin-R	5′-ATCCAACCGACTGCTGTCA-3′
3	Human-β-actin -F	5′- CACCATTGGCAATGAGCGGTTC-3′
4	Human-β-actin -R	5′- AGGTCTTTGCGGATGTCCACGT-3′
5	Bovine-RBMX2-F	5′-TCCCACCGGCACAAAAAGTC-3′
6	Bovine-RBMX2-R	5′-TCAGTGATACCTGAGCTCCC-3′
7	Human-RBMX2-F	5′-ACCCCCTCACCAAGTTTGTC-3′
8	Human-RBMX2-R	5′-GTGCTTCTTAGGGCCAGTGT-3′
9	Bovine-HSPB8-F-1	5′-GACCAAGGACGGATACGTGG-3′
10	Bovine-HSPB8-R-1	5′-AGTTCTTGGAGACGATGCCC-3′
11	Bovine-ST14-F-1	5′-CTCGGCGCTGGATTCAAGTA-3′
12	Bovine-ST14-R-1	5′-CAAGAACTCCACGCCTTCCT-3′
13	Bovine-MUC16-F-1	5′-TGTGCATGTGACAGCAGAGC-3′
14	Bovine-MUC16-R-1	5′-CTGGAAACTGGGAGTGGTCG-3′
15	Bovine-TNC-F-1	5′-TGGCATCGGAGAATGCCTTT-3′

16	Bovine-TNC-R-1	5′-CAGCTTCCTCTGGGTTCCTG-3′
17	Bovine-GPX2-F-1	5′-ACCCGTTTTCCCTCATGACC-3′
18	Bovine-GPX2-R-1	5′-CGGCCCAATGAGGAACTTCT-3′
19	Bovine-THBS2-F-1	5′-GGGGACGCTTGTAAAGACGA-3′
20	Bovine-THBS2-R-1	5′-AATCTGAGTGGTGCCCTTGG-3′
21	Bovine-IL-7-F-1	5′-GCAATTGCCTGAATAACGAACCT-3′
22	Bovine-IL-7-R-1	5′-TTACCCTTGCTGGTGCAGTT-3′
23	Bovine-IL-24-F-1	5′-GACGCCTGCCCAACTTTCTT-3′
24	Bovine-IL-24-R-1	5′-AAGGGATGCTTGAGGGCTTG-3′
25	Bovine-FRMD4B-F-1	5′-CAGAGACAGGAGCACCAAGG-3′
26	Bovine-FRMD4B-R-1	5′-TTAAACTGCCGTTGCTTGCC-3′
27	Bovine-OMD-F-1	5′-GCTCAACGTTGGACACAACA-3′
28	Bovine-OMD-R-1	5′-AGCTTATTGGCGCTTTCAGC-3′
29	Bovine-NOS3-F-1	5′-GTTCCCTCGCGTGAAGAACT-3′
30	Bovine-NOS3-R-1	5′-CTGGTTGATGAAGTCCCTGGC-3′
31	Bovine-MCTP1-F-1	5′-AGTTCCGACTTGGGCATCAG-3′
32	Bovine-MCTP1-R-1	5′-TACTGAGAGCCGACAGGTCA-3′
33	Bovine-MFAP5-F-1	5′-TGATATCCAGCCTTCCACCG-3′
34	Bovine-MFAP5-R-1	5′-CCGATGCACGGAGTAGAGTC-3′
35	Bovine-MMP-9-1-F	5′-CGCTATGGCTACACTCCTGG-3′
36	Bovine-MMP-9-1-R	5′-TGAGTTCGCCCTCAAAGGTC-3′
37	Bovine-N-cadherin-1-F	5′-CACTGCGATTGATGCTGACG-3′
38	Bovine-N-cadherin-1-R	5′-TGCCACCGTGATAATGTCCC-3′
39	Bovine-E-cadherin 1-F	5′-CAGAAGATGACACCCGGGAC-3′
40	Bovine-E-cadherin 1-R	5′-AGCATCCAGGCCCCTATGTA-3′
41	Bovine-CLDN-5-F-1	5′-CCTGGACCACAACATCGTGA-3′
42	Bovine-CLDN-5-R-1	5′-GGAGTCGTACACCTTGCACT-3′
43	Bovine-OCLN-F-1	5′-CTTTCAAAAAGGGCTCCCGC-3′

44	Bovine-OCLN-R-1	5′-TGGATATTCCCTGATCCAGTCG-3′
45	Bovine-TJP1-F-1	5′-CTCAAGTTCCTGAAGCCCGT-3′
46	Bovine-TJP1-R-1	5′-TAGGATCACCCGACGAGGAG-3′
47	Bovine-TNF-F-1	5′-GAAGTTGCTTGTGCCTCAGC-3′
48	Bovine-TNF-R-1	5′-AACCAGAGGGCTGTTGATGG-3′
49	Bovine-IL-6-F-1	5′-CTTCTGCTTTCCCTACCCCG-3′
50	Bovine-IL-6-R-1	5′-TTCTGCCAGTGTCTCCTTGC-3′
51	Bovine-IL-1β-F-1	5′-AAAAGCTTCAGGCAGGTGGT-3′
52	Bovine-IL-1β-R-1	5′-AACTCGTCGGAGGACGTTTC-3′

Western blot

RIPA reagent (Sigma, USA), supplemented with protease inhibitors and phosphatase inhibitors (Roche, China), was added to the cell samples, and the cells were lysed on ice for 30 minutes. The supernatant was collected by centrifugation at 12,000 rpm and 4°C for 10 minutes. Protein concentrations of each sample were determined using a BCA kit (Beyotime, China), and the proteins were adjusted to equal concentrations.

The protein samples were mixed with 5× protein loading buffer and boiled for 10 minutes. Proteins were then separated using SDS-PAGE on 10% polyacrylamide gels at 100 V for 90 minutes, followed by transfer to polyvinylidene difluoride (PVDF) membranes (Millipore, Germany) at 100 V for 70 minutes. The PVDF membrane was incubated in 5% skimmed milk for 4 hours to block non-specific binding. The membrane was washed three times with Tris-buffered saline containing 0.15% Tween-20 (TBST) for 5 minutes each.

Subsequently, the membrane was incubated with a primary antibody at 4°C for 12 hours, followed by a secondary antibody at room temperature for 1 hour. The following primary antibodies were utilized: ZO-1 (Bioss, China), OCLN (Proteintech, China), CLADN-5 (Proteintech, China), MMP-9 (Proteintech, China), E-cadherin (Proteintech, China), N-cadherin (Bioss, China), LaminA/C (Proteintech, China), β-actin (Bioss, China), p65 (CST, USA), p-p65 (CST, USA), and a MAPK-related antibody (CST, USA). The following secondary antibodies were used: anti-mouse

660 HRP secondary antibody and anti-rabbit HRP (Invitrogen, USA).

661

662 Phylogenetic tree construction and gene structure and function predictive analysis of the
663 bovine RBM family

664 The bovine RBM protein sequences were converted into FASTA format files and imported
665 into MEGA-X for comparative analysis. The neighbor-joining method was employed to construct
666 the phylogenetic tree of the CsGRF protein. The iTOL website (https://itol.embl.de/) was utilized
667 to enhance the visualization of the CsGRF phylogenetic tree. Additionally, the MEME Suite
668 database (http://meme-suite.org/) was used for the online analysis of conserved motifs within
669 the RBM gene family.

670

671 Adhesion Assay

672 EBL cells were infected with different live bacteria at a multiplicity of infection (MOI) of 20
673 for durations of 15 minutes, 30 minutes, 1 hour, and 2 hours at 4°C. Following infection, the cells
674 were washed three times with phosphate-buffered saline (PBS; Gibco, USA) to remove
675 extracellular bacteria. After washing, cells were lysed using 0.1% Triton X-100 (Beyotime, China).
676 The resulting lysates were plated onto 7H11 or LB agar plates and incubated for several days to
677 enable enumeration of colony-forming units (CFUs).

678

679

680 Invasion Assay

681 EBL cells were infected with various live bacteria at an MOI of 20 for durations of 2, 4, and 6
682 hours at 37 °C. After infection, gentamicin (Procell, China) was added at a concentration of 100
683 μg/mL for 2 hours to eliminate extracellular bacteria. The infected cells were then washed three
684 times with phosphate-buffered saline (PBS; Gibco, USA) to remove residual extracellular bacteria.
685 Following thorough washing, the cells were lysed using 0.1% Triton X-100 (Beyotime, China). The
686 resulting lysates were plated onto 7H11 or LB agar plates and incubated for several days to allow
687 for colony-forming unit (CFU) enumeration.

688

689 Intracellular Survival Assay

690 EBL cells were infected with various live bacterial strains at a multiplicity of infection (MOI)
691 of 20 for 6 hours at 37°C. After infection, extracellular bacteria were removed by treating the cells
692 with gentamicin (100 μg/mL; Procell, China) for 2 hours. The infected cells were then washed
693 three times with phosphate-buffered saline (PBS; Gibco, USA) to eliminate any remaining
694 extracellular bacteria, marking the 0-hour time point.

695 Following this, the infected cells were cultured in complete medium supplemented with
696 0.1% Triton X-100 (Beyotime, China) and harvested at selected time points: 0, 24, 48, and 72
697 hours post-infection (hpi). Cell lysates were plated onto 7H11 or LB agar plates and incubated for
698 several days to allow for colony-forming unit (CFU) enumeration.

699

700 RNA-Seq, proteomics and metabolomics

701 We collected cells at different time points after infection, where the cells at 0 hours were
702 treated with gentamicin 2 hours post-infection with *M. bovis* to eliminate extracellular bacteria.
703 Total RNA was isolated using Trizol Reagent (Invitrogen Life Technologies), and the concentration,
704 quality, and integrity were determined using a NanoDrop spectrophotometer (Thermo Scientific).
705 Three micrograms of RNA were used as input material for RNA sample preparation. Sequencing
706 libraries were generated according to the following steps: mRNA was purified from total RNA
707 using poly-T oligo-attached magnetic beads. Fragmentation was performed using divalent cations
708 under elevated temperature in an Illumina proprietary fragmentation buffer. First-strand cDNA
709 was synthesized using random oligonucleotides and Super Script II. Second-strand cDNA synthesis
710 was subsequently performed using DNA Polymerase I and RNase H. The remaining overhangs
711 were converted into blunt ends via exonuclease/polymerase activities, and the enzymes were
712 removed. After adenylation of the 3' ends of the DNA fragments, Illumina PE adapter
713 oligonucleotides were ligated for hybridization. To select cDNA fragments of the preferred length
714 of 400–500 bp, the library fragments were purified using the AMPure XP system (Beckman
715 Coulter, Beverly, CA, USA). DNA fragments with ligated adaptor molecules at both ends were
716 selectively enriched using the Illumina PCR Primer Cocktail in a 15-cycle PCR reaction. The
717 products were purified (AMPure XP system) and quantified using the Agilent high-sensitivity DNA

assay on a Bioanalyzer 2100 system (Agilent). The sequencing library was then sequenced on the NovaSeq 6000 platform (Illumina) by Shanghai Personal Biotechnology Co., Ltd.

RNA sequencing services were provided by Personal Biotechnology Co., Ltd. Shanghai, China. The data were analyzed using the free online platform Personalbio GenesCloud (https://www.genescloud.cn). Proteomics and metabolomics were performed by METWARE.

Differential expression analysis of the transcriptome

The statistical methods of HTSeq (0.9.1) RRID:SCR_005514 were used to compare read count values for each gene, which served as raw measurements of gene expression, while FPKM (Fragments Per Kilobase of transcript per Million mapped reads) was used for data normalization. Subsequently, differential gene expression analysis was performed using DESeq (1.30.0) RRID:SCR_000154 under the following screening criteria: |log2FoldChange| > 2 indicated a significant fold change in expression, and a P-value < 0.05 was considered statistically significant. The resulting list of differentially expressed genes was used for further functional enrichment and pathway analysis.

For clustering analysis of differentially expressed genes, the Pheatmap (1.0.8) package in R was used to perform bidirectional clustering analysis on the expression patterns of all differentially expressed genes across various samples. The heatmap was constructed based on the expression levels of the same gene across different samples and the expression patterns of different genes within the same sample. Distance calculations were based on Euclidean distance, and complete linkage clustering was used to visualize overall expression differences among samples and similarities in gene expression patterns.

Moreover, to further enhance the flexibility and reproducibility of data analysis, a localized analysis workflow was introduced. All raw sequencing data (FASTQ files) underwent quality control (using FastQC) and were aligned (using STAR or HISAT2) to the reference genome, followed by gene expression quantification and differential analysis using locally installed HTSeq and DESeq2 pipelines. This local workflow not only improves the transparency and controllability of data processing but also enhances data privacy protection, making it particularly suitable for handling sensitive or large-scale datasets. All analysis parameters were thoroughly documented

747 to ensure experimental reproducibility and result traceability.

748 Finally, data analysis was also supported by the free online analytical platform Personalbio
749 GenesCloud (https://www.genescloud.cn), which provides a graphical interface and efficient
750 cloud computing resources, supporting differential analysis, functional annotation (GO/KEGG),
751 gene set enrichment analysis (GSEA), and visualization. The results from local and cloud-based
752 analyses complement each other, ensuring comprehensive and accurate data interpretation.

753

754 GO and KEGG enrichment analysis

755 We mapped all genes to terms in the Gene Ontology (GO) database and calculated the
756 number of differentially enriched genes for each term. GO enrichment analysis was conducted on
757 the differentially expressed genes using the topGO package, where P-values were determined
758 using the hypergeometric distribution method. A threshold of P-value < 0.05 was set to identify
759 significant enrichment, allowing us to pinpoint GO terms associated with significantly enriched
760 differential genes and to elucidate the primary biological functions they perform. Additionally, we
761 employed ClusterProfiler (3.4.4) software to conduct KEGG pathway enrichment analysis for the
762 differential genes, concentrating on pathways with a P-value < 0.05. The data analysis was carried
763 out using the free online platform Personalbio GenesCloud (https://www.genescloud.cn).

764

765 Flow cytometry assay

766 Cells were washed with cold PBS and then centrifuged at 1,500 rpm for 5 minutes; the
767 supernatant was discarded. The cells were fixed in 70% ethanol for 12 hours. Following fixation,
768 the cells were centrifuged again at 1,500 rpm for 5 minutes, and the supernatant was removed.
769 The cells were washed once with cold PBS.

770 For staining, a Cell Cycle and Apoptosis Analysis Kit (Beyotime, China) was utilized. The
771 staining mixture was prepared with a total volume of 535 μL, comprising 500 μL of staining buffer,
772 25 μL of PI dye, and 10 μL of RNase A. The samples were incubated with the staining mixture at
773 37°C for 30 minutes prior to detection.

774

775

776 Cell viability assay

777 EBL cells were infected with *M. bovis* at an MOI of 100. Cell viability was assessed at 48, 72,
778 96, 120, and 144 hpi using the CCK-8 assay (Dojindo, Kumamoto, Japan).

779 At each time point, fresh medium containing 10% CCK-8 was added to a 96-well cell plate
780 and incubated for 60 minutes at 37°C. The cell viability was then determined by measuring the
781 absorbance at 450 nm. The percentage of cell viability was calculated using the following
782 formula:

783 cell viability (%) = [A (infection group) − A (blank group)] / [A (infection group) A (blank
784 group)] × 100

785

786 Wound-Healing Assay

787 A wound-healing assay was performed to evaluate the migratory capacity of treated cells
788 following experimental intervention. Briefly, after a 48-hour co-culture of EBL cells with BoMac
789 cells post-M. bovis infection, the cells were harvested and dissociated using 1x trypsin.
790 Approximately 2 x 10^5 cells were then seeded into each well of a 6-well culture plate and allowed
791 to adhere until they reached confluence and formed a uniform monolayer.

792 Once a confluent cell monolayer was achieved, a standardized "wound" was created by
793 gently scratching the surface of the monolayer along a straight edge using a 200 µL pipette tip. To
794 remove non-adherent and detached cells, the monolayer was rinsed three times with
795 phosphate-buffered saline (PBS, Gibco, USA). Subsequently, serum-free culture medium was
796 added to each well to minimize cell proliferation and to better assess cell migration.

797 Phase-contrast images of the wound area were captured at defined time points-0, 12, and
798 24 hours-using an inverted microscope. The wound closure rate was quantitatively analyzed using
799 ImageJ software by measuring the change in wound width over time. The percentage of wound
800 healing was calculated relative to the initial wound width at time 0.

801 This assay provided insights into the effects of M. bovis infection and subsequent treatments
802 on cell migration, a critical component of the wound-healing process.

803

804

805 Cell Adhesion Assay

806 To evaluate the impact of RBMX2 knockout on the adhesive properties of EBL cells following
807 M. bovis infection, a cell adhesion assay was performed using a commercially available cell
808 adhesion detection kit (Bestbio, China), following the manufacturer’s instructions.

809 Matrigel (20 mg/L), used to simulate an extracellular matrix environment, was coated onto
810 the wells of a 96-well plate at a volume of 100 μL per well. Subsequently, 3 x10^4 cells (from
811 either RBMX2 knockout or wild-type (WT) EBL cell lines) were seeded into each well and
812 incubated for 6 hours in a CO_2 incubator at 37°C to allow cell attachment.

813 Following incubation, non-adherent cells were gently removed by washing the wells twice
814 with phosphate-buffered saline (PBS). Adherent cells were then fixed and stained with 10 μL of
815 cell stain solution A per well and incubated for an additional 2 hours at 37 °C.

816 The absorbance was measured at 560 nm using a microplate reader to quantify the intensity
817 of staining, which correlates with the number of adhered cells. The results were used to compare
818 the adhesive capacities of RBMX2 knockout versus wild-type EBL cells under the experimental
819 conditions.

820 This assay provided a quantitative assessment of cell-matrix adhesion, offering insights into
821 the potential role of RBMX2 in modulating cell adhesion during M. bovis infection.

822

823 Transwell Assay

824 To evaluate the migratory and invasive potential of treated EBL cells, a Transwell assay was
825 performed using Transwell chambers (Corning, USA). A total of 5 x 10^4 cells suspended in 200
826 μL of serum-free culture medium were seeded into the upper chamber, while 550 μL of complete
827 medium containing fetal bovine serum was added to the lower chamber to serve as a
828 chemoattractant.

829 The cells were allowed to migrate through the membrane for 24 hours in a CO_2 incubator at
830 37 °C.

831 Following incubation, the Transwell insert was carefully removed, and the cells on the upper
832 surface of the membrane were gently wiped away with a cotton swab. The migrated cells on the
833 lower surface were then fixed by incubation with 550 μL of 4% paraformaldehyde (Beyotime,

834 China) for 30 minutes at room temperature. After fixation, the cells were stained with 550 µL of
835 crystal violet solution (Beyotime, China) for an additional 30 minutes to allow for visualization of
836 the migrated cells.

837 The stained membrane was rinsed briefly with PBS for 30 seconds to remove excess dye,
838 air-dried upside down, and then carefully removed from the insert. It was subsequently mounted
839 onto a glass slide and sealed with neutral balsam to preserve the staining.

840 Images were captured under a light microscope, and three random fields of view were
841 selected for analysis. The number of migrated cells was quantified using ImageJ software
842 (RRID:SCR_003070). The results were used to compare the migratory abilities of different
843 experimental groups.

844 This assay provided a quantitative assessment of cell migration, which is essential for
845 understanding the functional impact of treatments or genetic modifications on cell motility.

846

847 Crystal violet staining assay

848 EBL cells were infected with *M. bovis* at an MOI of 100. The surviving cells on six-well plates
849 were then fixed with 4% paraformaldehyde (Beyotime, China). After fixation, the cells were
850 stained with 0.1% crystal violet staining solution (Beyotime, China) and rinsed five times with PBS
851 (Gibco, USA). The plates were placed in a 37°C oven for 6 hours before being photographed.

852

853 *M. bovis* infection of BoMac and coculture with EBL cells

854 BoMac cells were seeded into the upper chamber of a 0.4 µm pore size Transwell (Corning,
855 USA) at a density of 3×10^4 cells per insert in RPMI 1640 medium supplemented with 10% FBS.
856 The following day, the cells were infected with *M. bovis* at an MOI of 5 for 4 hours. After infection,
857 the cells were washed three times with 1× warm PBS and treated with Gentamycin (100 µg/mL)
858 for 2 hours to eliminate any extracellular bacilli.

859 The infected and uninfected BoMac cells were then incubated for 24 hours to mitigate the
860 effects of *M. bovis* infection. Afterward, the cells underwent an additional 24-hour incubation
861 period in fresh RPMI 1640 medium before coculturing with EBL cells.

862 In parallel, EBL cells were seeded at a density of 2×10^5 cells per well onto 12-well plates

863 containing DMEM supplemented with 10% FBS. The following day, culture inserts containing
864 either *M. bovis*-infected or uninfected BoMac cells were introduced into the wells of the 12-well
865 plates containing EBL cells, and the coculture was incubated for up to 24 and 48 hours in
866 serum-free DMEM.
867
868 Small interfering RNA (siRNA) transfection
869 EBL cells were transfected with p65 siRNA (Tsingke, China) using jetPRIME (Polyplus, France)
870 following the manufacturer's instructions. Scrambled siRNA (Tsingke, China) served as a negative
871 control.
872 Cells were seeded in 12-well plates and cultured at 37°C in a 5% CO_2 atmosphere. To prepare
873 the transfection mixture, 0.8 μg of jetPRIME was incubated with 1 μL of siRNA for 10 minutes.
874 This mixture was then added to the cells and incubated for 12 hours.
875 Following the incubation, RNA extraction was performed, and the efficiency of transfection
876 was calculated.
877 The siRNA sequences used were as follows:
878 Cattle p65-1 siRNA, sense 5'-GCAGUUUGAUACCGAUGAA (dT)(dT)-3';
879 Cattle p65-1 siRNA, antisense 5'-UUCAUCGGUAUCAAACUGC (dT)(dT)-3';
880 Cattle p65-2 siRNA, sense 5'-GGACGUACGAGACCUUCAA (dT)(dT)-3';
881 Cattle p65-2 siRNA, antisense 5'-UUGAAGGUCUCGUACGUCC (dT)(dT)-3'.
882
883 P65 nuclear translocation assay
884 For the p65 nuclear translocation assay, RBMX2 knockout and wild-type cell lines were
885 transfected with the pCMV-EGFP-p65 plasmid. Following transfection, bovine lung epithelial cells
886 were infected with *M. bovis*.
887 After infection, the cell nuclei were stained with Hoechst dye. The entry of p65 into the
888 nucleus was analyzed at different time points using a confocal high-resolution cell imaging
889 analysis system from PerkinElmer Life and Analytical Sciences Ltd. (Britain). This imaging
890 technique allowed for the assessment of p65 translocation into the nucleus in response to
891 infection.

892

893 CHIP-PCR

894 Formaldehyde cross-linking and ultrasonic fragmentation of cells were performed. One plate
895 of cells was removed, and the volume of the culture medium was measured. 37% formaldehyde
896 was added to achieve a final concentration of 1%, and the plates were incubated at 37°C for 10
897 minutes. Glycine (2.5 M) was then added to the plates at a final concentration of 125 mM to
898 terminate cross-linking. After mixing, the culture medium was left at room temperature for 5
899 minutes, and the cells were cleaned three times with cold PBS. The cells were scraped off with
900 PBS, centrifuged at 2,000g for 5 minutes, and the supernatant was removed. IP lysis solution
901 containing a protease inhibitor was added to lyse the cells (the amount of lysis solution
902 depending on the amount of cell precipitation), and the mixture was fully lysed on ice for 30
903 minutes, with the cells being repeatedly blown with a gun or shaken on a vortex mixer to ensure
904 complete lysis.

905 After sonication, the mixture was centrifuged at 12,000 rpm at 4°C for 10 minutes to remove
906 insoluble substances and collect the supernatant. 90 μL of the input was retained, and the rest
907 was stored at −80°C. To confirm the presence of the target protein in the sample, 40 μL of the
908 ultrasonic crushing product was taken, mixed with 10 μL of L5 reduced protein loading buffer, and
909 heated for denaturation before performing Western blot detection.

910 For the remaining 50 μL of the product, 5 μL of Protease K and 2 μL of 5M NaCl (final NaCl
911 concentration of 0.2M) were added and incubated at 55°C overnight for cross-linking. After
912 cross-linking, the nucleic acid concentration was measured, and a portion of the sample was
913 taken for PCR amplification, followed by agarose gel electrophoresis to detect the effectiveness of
914 ultrasonic fragmentation and confirm the presence of the target DNA. After verifying the Input
915 result, 100 μL of the ultrasonic crushing products was frozen at −80°C.

916 Next, 900 μL of ChIP Diffusion Buffer containing 1 mM PMSF and 20 μL of 50% of 1× PIC was
917 added, along with an additional 60 μL of Protein A+G Agarose/Salmon Sperm DNA. The mixture
918 was stirred at 4°C for 1 hour, allowed to stand at 4°C for 10 minutes to precipitate, and then
919 centrifuged at 4000 rpm for 5 minutes. The sample was divided into two 1.5 mL EP tubes; the
920 target protein IP antibody was added to one tube, while IgG (1 μg of the corresponding species)

921 was added to the other. The samples were shaken overnight at 4°C for precipitation and cleaning
922 of immune complexes.

923 After the overnight incubation, 200 μL of Protein A+G Agarose/Salmon Sperm DNA was
924 added to each tube, shaken at 4°C for 2 hours, allowed to stand at 4°C for 10 minutes, and then
925 centrifuged at 4,000 rpm for 1 minute. The supernatant was removed, and 8 μL of 5M NaCl and
926 20 μL of Protein K were added for overnight cross-linking at 55°C. Using databases like JASPAR to
927 predict transcription factor binding sites, primers were designed and synthesized based on these
928 binding sites. RT-PCR was employed to verify the binding, and after amplification, the products
929 were taken for gel electrophoresis to confirm the correct fragment size (Table S3).

930 Table S3

Gene name	Sequence
MMP9	5′-AGGCACTGAAGGAATGAGGC-3′
	5′-CCCCGCTTGGTGGAAAT-3′
RBMX2	5′-CTGACAGGAGGACCAGAGTTT-3′
	5′-TGCCTAGTTGTAGGGTTGAAGT-3′

931

932 Dual-luciferase reporter assay

933 293T cells in the logarithmic growth phase were adjusted to a density of 5×10^4 cells/mL and
934 inoculated into 48-well cell culture plates, with 300 cells per well. Each concentration gradient
935 was represented by three replicate wells. On the second day after plating, when the cells reached
936 a density of approximately 60-70%, transfection was performed with the following experimental
937 groups: pGL4.10 RRID:Addgene_72684 basic+pRL TK+Over NC, pGL4.10 basic+pRL TK+Over p65,
938 pGL4.10-*RBMX2*-WT+pRL TK+Over NC, pGL4.10-*RBMX2*-WT+pRL TK+Over p65,
939 pGL4.10-*RBMX2*-MUT+pRL TK+Over NC, pGL4.10-*RBMX2*-MUT+pRL TK+Over p65. Transfection
940 complexes were prepared, and dual-luciferase detection was carried out 48 hours
941 post-transfection.

942 For cell lysis, the cell culture medium was removed, and the cells were gently rinsed twice
943 with PBS. Then, 50 μL of 1× PLB lysis solution was added to each well, and the plates were placed
944 on a shaking table at room temperature for 15 minutes to ensure complete lysis.

945 From each sample, 20 μL was taken for measurement. To assess Firefly luciferase activity,
946 100 μL of Firefly luciferase detection reagent (LAR II reagent, Promega, USA) was added, mixed
947 well, and the relative light unit (RLU1) was measured. After this, 100 μL of Sea Kidney luciferase
948 detection reagent (1× Stop&Glo® Reagent, Promega, USA) was added, mixed thoroughly, and the
949 relative light unit (RLU2) was measured.
950 The activation level of the target reporter genes was compared between different samples
951 by calculating the ratio of RLU1 from the Firefly luciferase assay to RLU2 from the Sea Kidney
952 luciferase assay.
953
954 Protein docking
955 Molecular docking simulations were conducted to predict the formation of stable complexes
956 between proteins RBMX2 or MMP9 with p65. The aligned sequences of RBMX2, MMP9, and p65
957 proteins were sourced from the UniProt RRID:SCR_002380 database. Their three-dimensional
958 structures were predicted using AlphaFold and refined by constructing the structures in Avogadro.
959 The structures were then optimized using the MMFF94 force field and exported in PDB format for
960 further optimization in Gauss09.
961 The docking of the proteins was performed using Hdock, where each protein was treated
962 separately as the receptor and ligand to assess their interactions [81]. The resulting docking
963 affinities were annotated to provide insight into the binding interactions. Finally, PyMOL
964 RRID:SCR_000305 was utilized to visualize the binding interaction geometries, allowing for a
965 detailed examination of the molecular interactions between the proteins.
966
967 Statistical analysis
968 Statistical analysis was performed on all assays conducted in triplicate, with data expressed
969 as the mean ± standard error of the mean. Each experiment was independently repeated three
970 times. GraphPad Prism 7.0 RRID:SCR_002798 (La Jolla) was utilized for statistical analysis,
971 employing a two-tailed unpaired t-test with Welch's correction for comparisons between two
972 groups. For comparisons among multiple groups, one-way or two-way ANOVA was applied,
973 followed by the LSD test. Statistical significance was indicated at four levels: not significant (ns

presents $p > 0.05$), * presents $p < 0.05$, ** presents $p < 0.01$, and *** presents $p < 0.001$.

Acknowledgments

We would like to thank the National Key Laboratory of Agricultural Microbiology Core Facility for assistance in high-throughput microscopy, and we are grateful to Zhe Hu for his support of the sample preparation. This work was supported by the Major projects of agricultural biological breeding in China (2023ZD0405003), the National Natural Science Foundation of China (32072942), China Agriculture Research System of MOF and MARA (CARS-37), National Natural Science Foundation of China (81960772) and Key Project of Inner Mongolia Medical University (YKD2022ZD016).

Author Contributions

YC and AG contributed to the conception and design of the study. CW, YP and HY carried out the experiment and wrote sections of the manuscript and made equal contribution. YJ, AK, ZY, KZ, and SX were involved in bacterial and cell research studies. CW, YP, HY, SX, LB, LZ, YY, and HC performed the statistical analysis. CW, AG, and YC wrote the manuscript with all authors providing feedback. All authors contributed to manuscript revision, proof-reading, and approval of the submitted version.

Conflict of Interest

The authors declare that the research was conducted in the absence of any commercial or financial relationships that could be construed as a potential conflict of interest.

References

1. WHO, *Global tuberculosis report*. 2023.
2. Preda, M.; Tănase, B. C.; Zob, D. L.; Gheorghe, A. S.; Lungulescu, C. V.; Dumitrescu, E. A.; Stănculeanu, D. L.; Manolescu, L. S. C.; Popescu, O.; Ibraim, E.; Mahler, B., The Bidirectional Relationship between Pulmonary Tuberculosis and Lung Cancer. *Int J Environ Res Public Health* 2023, *20* (2).
3. Cabrera-Sanchez, J.; Cuba, V.; Vega, V.; Van der Stuyft, P.; Otero, L., Lung cancer occurrence after an episode of tuberculosis: a systematic review and meta-analysis. *Eur Respir Rev* 2022, *31* (165).
4. Suarez-Carmona, M.; Lesage, J.; Cataldo, D.; Gilles, C., EMT and inflammation: inseparable actors of cancer progression. *Mol Oncol* 2017, *11* (7), 805-823.
5. Wang, C.; Jiang, Y.; Yang, Z.; Xu, H.; Khalid, A. K.; Iftakhar, T.; Peng, Y.; Lu, L.; Zhang, L.; Bermudez, L.; Guo, A.; Chen, Y., Host factor RBMX2 promotes epithelial cell apoptosis by downregulating APAF-1's Retention Intron after Mycobacterium bovis infection. *Front Immunol* 2024, *15*, 1431207.
6. Song, Y.; He, S.; Ma, X.; Zhang, M.; Zhuang, J.; Wang, G.; Ye, Y.; Xia, W., RBMX contributes to hepatocellular carcinoma progression and sorafenib resistance by specifically binding and stabilizing BLACAT1. *Am J Cancer Res* 2020, *10* (11), 3644-3665.
7. Schümann, F. L.; Bauer, M.; Groß, E.; Terziev, D.; Wienke, A.; Wickenhauser, C.; Binder, M.; Weber, T., RBMX Protein Expression in T-Cell Lymphomas Predicts Chemotherapy Response and Prognosis. *Cancers (Basel)* 2021, *13* (19).
8. Alors-Pérez, E.; Blázquez-Encinas, R.; Moreno-Montilla, M. T.; García-Vioque, V.; Jiménez-Vacas, J. M.; Mafficini, A.; González-Borja, I.; Luchini, C.; Sánchez-Hidalgo, J. M.; Sánchez-Frías, M. E.; Pedraza-Arevalo, S.; Romero-Ruiz, A.; Lawlor, R. T.; Viúdez, A.; Gahete, M. D.; Scarpa, A.; Arjona-Sánchez, Á.; Luque, R. M.; Ibáñez-Costa, A.; Castaño, J. P., Spliceosomic dysregulation in pancreatic cancer uncovers splicing factors PRPF8 and RBMX as novel candidate actionable targets. *Mol Oncol* 2024, *18* (10), 2524-2540.
9. Wibbe, N.; Ebnet, K., Cell Adhesion at the Tight Junctions: New Aspects and New Functions. *Cells-Basel* 2023, *12* (23).
10. Bhat, A. A.; Uppada, S.; Achkar, I. W.; Hashem, S.; Yadav, S. K.; Shanmugakonar, M.; Al-Naemi, H. A.; Haris, M.; Uddin, S., Tight Junction Proteins and Signaling Pathways in Cancer and Inflammation: A Functional Crosstalk. *Front Physiol* 2018, *9*, 1942.
11. Zou, Y.; Xiang, Q.; Wang, J.; Peng, J.; Wei, H., Oregano Essential Oil Improves Intestinal Morphology and Expression of Tight

Junction Proteins Associated with Modulation of Selected Intestinal Bacteria and Immune Status in a Pig Model. *Biomed Res Int* 2016, *2016*, 5436738.

12. Edelblum, K. L.; Turner, J. R., The tight junction in inflammatory disease: communication breakdown. *Curr Opin Pharmacol* 2009, *9* (6), 715-20.

13. Bell, C. E.; Watson, A. J., p38 MAPK regulates cavitation and tight junction function in the mouse blastocyst. *PLoS One* 2013, *8* (4), e59528.

14. Kitagawa, N.; Inai, Y.; Higuchi, Y.; Iida, H.; Inai, T., Inhibition of JNK in HaCaT cells induced tight junction formation with decreased expression of cytokeratin 5, cytokeratin 17 and desmoglein 3. *Histochem Cell Biol* 2014, *142* (4), 389-99.

15. Lin, X.; Zhu, Y.; Le, G., Tetramethylpyrazine Alleviates Tight Junction Disruption of Bronchial Mucosal Epithelial Cells Caused by Interleukin-17 via Inhibiting Nuclear Factor-κB-p65/Tumor Necrosis Factor-α Signaling Pathway. *J Interferon Cytokine Res* 2021, *41* (11), 415-424.

16. Jeong, C. H.; Seok, J. S.; Petriello, M. C.; Han, S. G., Arsenic downregulates tight junction claudin proteins through p38 and NF-κB in intestinal epithelial cell line, HT-29. *Toxicology* 2017, *379*, 31-39.

17. Singh, V.; Phukan, U. J., Interaction of host and Staphylococcus aureus protease-system regulates virulence and pathogenicity. *Med Microbiol Immunol* 2019, *208* (5), 585-607.

18. Gu, L.; Wang, H.; Guo, Y. L.; Zen, K., Heparin blocks the adhesion of E. coli O157:H7 to human colonic epithelial cells. *Biochem Biophys Res Commun* 2008, *369* (4), 1061-4.

19. Harrandah, A. M.; Chukkapalli, S. S.; Bhattacharyya, I.; Progulske-Fox, A.; Chan, E. K. L., Fusobacteria modulate oral carcinogenesis and promote cancer progression. *J Oral Microbiol* 2021, *13* (1).

20. Li, N. S.; Xu, X. B.; Yang, H.; Wang, H.; Ouyang, Y. B.; Zhou, Y. A.; Peng, C.; Yuan, Z. X.; He, C.; Zeng, C. Y.; Hong, J. B., Activation of Aquaporin 5 by carcinogenic infection promotes epithelial-mesenchymal transition via the MEK/ERK pathway. *Helicobacter* 2021, *26* (5).

21. Bessède, E.; Dubus, P.; Mégraud, F.; Varon, C., infection and stem cells at the origin of gastric cancer. *Oncogene* 2015, *34* (20), 2547-2555.

22. Ferluga, J.; Yasmin, H.; Al-Ahdal, M. N.; Bhakta, S.; Kishore, U., Natural and trained innate immunity against. *Immunobiology* 2020, *225* (3).

23. Strong, E. J.; Wang, J.; Ng, T. W.; Porcelli, S. A.; Lee, S., Mycobacterium tuberculosis PPE51 Inhibits Autophagy by Suppressing Toll-Like Receptor 2-Dependent Signaling. *Mbio* 2022, *13* (3).

24. Vignesh, R.; Balakrishnan, P.; Tan, H. Y.; Yong, Y. K.; Velu, V.; Larsson, M.; Shankar, E. M., Tuberculosis-Associated Immune Reconstitution Inflammatory Syndrome-An Extempore Game of Misfiring with Defense Arsenals. *Pathogens* 2023, *12* (2).

25. Certo, M.; Tsai, C. H.; Pucino, V.; Ho, P. C.; Mauro, C., Lactate modulation of immune responses in inflammatory versus tumour microenvironments. *Nat Rev Immunol* 2021, *21* (3), 151-161.

26. Harmon, C.; O'Farrelly, C.; Robinson, M. W., The Immune Consequences of Lactate in the Tumor Microenvironment. *Tumor Microenvironment: Molecular Players, Pt A* 2020, *1259*, 113-124.

27. Rodel, H. E.; Ferreira, I. A. T. M.; Ziegler, C. G. K.; Ganga, Y.; Bernstein, M.; Hwa, S. H.; Nargan, K.; Lustig, G.; Kaplan, G.; Noursadeghi, M.; Shalek, A. K.; Steyn, A. J. C.; Sigal, A., Aggregated Enhances the Inflammatory Response. *Front Microbiol* 2021, *12*.

28. Park, D. W.; Moon, S. M.; Choi, H.; Kim, S. H.; Kang, H. K.; Jung, J. H.; Han, K.; Shin, D. W.; Lee, H., Increased lung cancer risk and associated risk factors in tuberculosis survivors: a Korean population-based study. *Cancer Res* 2023, *83* (7).

29. Hu, M., A Case of Multi-Organ Tuberculosis Misdiagnosed as Lung Cancer and a Literature Review. *Cancer Manag Res* 2023, *15*, 1395-1400.

30. Menakuru, S.; Dhillon, V.; Emran, J.; Khan, I.; Beirat, A.; Salih, A., Are Delays In The Diagnosis Of Lung Cancer Due To Patients First Seeking Treatment for Tuberculosis In Rural India? *J Thorac Oncol* 2023, *18* (3), E23-E23.

31. Liu, W.; Wang, H.; Bai, F.; Ding, L.; Huang, Y.; Lu, C.; Chen, S.; Li, C.; Yue, X.; Liang, X.; Ma, C.; Xu, L.; Gao, L., IL-6 promotes metastasis of non-small-cell lung cancer by up-regulating TIM-4 via NF-κB. *Cell Prolif* 2020, *53* (3), e12776.

32. Shrestha, R.; Bridle, K. R.; Crawford, D. H. G.; Jayachandran, A., TNF-α-mediated epithelial-to-mesenchymal transition regulates expression of immune checkpoint molecules in hepatocellular carcinoma. *Mol Med Rep* 2020, *21* (4), 1849-1860.

33. Hao, Y.; Baker, D.; Ten Dijke, P., TGF-β-Mediated Epithelial-Mesenchymal Transition and Cancer Metastasis. *Int J Mol Sci* 2019, *20* (11).

34. Xu, G.; Li, Y.; Yang, J.; Zhou, X.; Yin, X.; Liu, M.; Zhao, D., Effect of recombinant Mce4A protein of Mycobacterium bovis on expression of TNF-alpha, iNOS, IL-6, and IL-12 in bovine alveolar macrophages. *Mol Cell Biochem* 2007, *302* (1-2), 1-7.

35. Na, T. Y.; Schecterson, L.; Mendonsa, A. M.; Gumbiner, B. M., The functional activity of E-cadherin controls tumor cell metastasis at multiple steps. *P Natl Acad Sci USA* 2020, *117* (11), 5931-5937.

36. Fedele, M.; Sgarra, R.; Battista, S.; Cerchia, L.; Manfioletti, G., The Epithelial-Mesenchymal Transition at the Crossroads between Metabolism and Tumor Progression. *Int J Mol Sci* 2022, *23* (2).

37. Alqurashi, Y. E.; Al-Hetty, H. R. A. K.; Ramaiah, P.; Fazaa, A. H.; Jalil, A. T.; Alsaikhan, F.; Gupta, J.; Ramírez-Coronel, A. A.; Tayyib, N. A.; Peng, H., Harnessing function of EMT in hepatocellular carcinoma: From biological view to nanotechnological standpoint. *Environ Res* 2023, *227*.

38. Mirzaei, S.; Saghari, S.; Bassiri, F.; Raesi, R.; Zarrabi, A.; Hushmandi, K.; Sethi, G.; Tergaonkar, V., NF-κB as a regulator of cancer metastasis and therapy response: A focus on epithelial-mesenchymal transition. *J Cell Physiol* 2022, *237* (7), 2770-2795.

39. O'Leary, K.; Shia, A.; Schmid, P., Epigenetic Regulation of EMT in Non-Small Cell Lung Cancer. *Curr Cancer Drug Tar* 2018, *18* (1), 89-96.

40. Stefani, C.; Miricescu, D.; Stanescu-Spinu, I. I.; Nica, R. I.; Greabu, M.; Totan, A. R.; Jinga, M., Growth Factors, PI3K/AKT/mTOR and MAPK Signaling Pathways in Colorectal Cancer Pathogenesis: Where Are We Now? *Int J Mol Sci* 2021, *22* (19).

41. Kim, B. K.; Kim, D. M.; Park, H.; Kim, S. K.; Hwang, M. A.; Lee, J.; Kang, M. J.; Byun, J. E.; Im, J. Y.; Kang, M.; Park, K. C.; Yeom, Y. I.; Kim, S. Y.; Jung, H.; Kweon, D. H.; Cheong, J. H.; Won, M., Synaptotagmin 11 scaffolds MKK7-JNK signaling process to promote stem-like molecular subtype gastric cancer oncogenesis. *J Exp Clin Canc Res* 2022, *41* (1).

42. Gonzalez-Avila, G.; Sommer, B.; García-Hernández, A. A.; Ramos, C., Matrix Metalloproteinases' Role in Tumor Microenvironment. *Tumor Microenvironment: Extracellular Matrix Components - Pt A* 2020, *1245*, 97-131.

43. Cox, T. R., The matrix in cancer. *Nat Rev Cancer* 2021, *21* (4), 217-238.

44. Kwaan, H. C.; Lindholm, P. F., Fibrin and Fibrinolysis in Cancer. *Semin Thromb Hemost* 2019, *45* (4), 413-422.

45. Mego, M.; Karaba, M.; Minarik, G.; Benca, J.; Sedláčková, T.; Tothova, L.; Vlkova, B.; Cierna, Z.; Janega, P.; Luha, J.; Gronesova, P.; Pindak, D.; Fridrichova, I.; Celec, P.; Reuben, J. M.; Cristofanilli, M.; Mardiak, J., Relationship between Circulating Tumor Cells, Blood Coagulation, and Urokinase-Plasminogen-Activator System in Early Breast Cancer Patients. *Breast J* 2015, *21* (2), 155-160.

46. Kim, J. H., Interleukin-8 in the Tumor Immune Niche: Lessons from Comparative Oncology. *Tumor Microenvironment: The Role of Interleukins, Pt A* **2020**, *1240*, 25-33.

47. Zuo, J. H.; Zhu, W.; Li, M. Y.; Li, X. H.; Yi, H.; Zeng, G. Q.; Wan, X. X.; He, Q. Y.; Li, J. H.; Qu, J. Q.; Chen, Y.; Xiao, Z. Q., Activation of EGFR promotes squamous carcinoma SCC10A cell migration and invasion via inducing EMT-like phenotype change and MMP-9-mediated degradation of E-cadherin. *J Cell Biochem* **2011**, *112* (9), 2508-17.

48. Peng, W.; Jiang, J.; Fu, J.; Duan, H.; Wang, J.; Duan, C., lncRNA GMDS-AS1 restrains lung adenocarcinoma progression via recruiting TAF15 protein to stabilize SIRT1 mRNA. *Epigenomics* **2023**, *15* (7), 417-434.

49. Reis, A. C.; Cunha, M. V., The open pan- genome architecture and virulence landscape of Mycobacterium bovis. *Microb Genomics* **2021**, *7* (10).

50. Fan, Y. L.; Wu, J. B.; Cheng, X. W.; Zhang, F. Z.; Feng, L. S., Fluoroquinolone derivatives and their anti-tubercular activities. *Eur J Med Chem* **2018**, *146*, 554-563.

51. Borkowska, D. I.; Napiórkowska, A. M.; Brzezinska, S. A.; Kozinska, M.; Zabost, A. T.; Augustynowicz-Kopec, E. M., From Latent Tuberculosis Infection to Tuberculosis. News in Diagnostics (QuantiFERON-Plus). *Pol J Microbiol* **2017**, *66* (1), 5-8.

52. Rastogi, N.; Zarin, S.; Alam, A.; Konduru, G. V.; Manjunath, P.; Mishra, A.; Kumar, S.; Nagarajaram, H. A.; Hasnain, S. E.; Ehtesham, N. Z., Structural and Biophysical properties of therapeutically important proteins Rv1509 and Rv2231A of Mycobacterium tuberculosis. *Int J Biol Macromol* **2023**, *245*.

53. Corleis, B.; Dorhoi, A., Early dynamics of innate immunity during pulmonary tuberculosis. *Immunol Lett* **2020**, *221*, 56-60.

54. Abebe, F., Crosstalk between Mycobacterium tuberculosis and the host cell. *Clin Exp Immunol* **2021**, *204* (1), 32-40.

55. Reuschl, A. K.; Edwards, M. R.; Parker, R.; Connell, D. W.; Hoang, L.; Halliday, A.; Jarvis, H.; Siddiqui, N.; Wright, C.; Bremang, S.; Newton, S. M.; Beverley, P.; Shattock, R. J.; Kon, M.; Lalvanl, A., Innate activation of human primary epithelial cells broadens the host response to in the airways. *Plos Pathog* **2017**, *13* (9).

56. Dorhoi, A.; Kaufmann, S. H. E., Perspectives on host adaptation in response to: Modulation of inflammation. *Semin Immunol* **2014**, *26* (6), 533-542.

57. Rajararna, M. V. S.; Ni, B.; Dodd, C. E.; Schlesinger, L. S., Macrophage immunoregulatory pathways in tuberculosis. *Semin Immunol* **2014**, *26* (6), 471-485.

58. D'Agnillo, F.; Walters, K. A.; Xiao, Y. L.; Sheng, Z. M.;

Scherler, K.; Park, J.; Gygli, S.; Rosas, L. A.; Sadtler, K.; Kalish, H.; Blatti, C. A.; Zhu, R. Q.; Gatzke, L.; Bushell, C.; Memoli, M. J.; O'Day, S. J.; Fischer, T. D.; Hammond, T. C.; Lee, R. C.; Cash, J. C.; Powers, M. E.; O'Keefe, G. E.; Butnor, K. J.; Rapkiewicz, A. V.; Travis, W. D.; Layne, S. P.; Kash, J. C.; Taubenberger, J. K., Lung epithelial and endothelial damage, loss of tissue repair, inhibition of fibrinolysis, and cellular senescence in fatal COVID-19. *Sci Transl Med* 2021, *13* (620).

59. Barros, B. C. S. C.; Almeida, B. R.; Barros, D. T. L.; Toledo, M. S.; Suzuki, E., Respiratory Epithelial Cells: More Than Just a Physical Barrier to Fungal Infections. *J Fungi* 2022, *8* (6).

60. Hu, Y.; Mu, H. S.; Deng, Z. P., RBM14 as a novel epigenetic-activated tumor oncogene is implicated in the reprogramming of glycolysis in lung cancer. *World J Surg Oncol* 2023, *21* (1).

61. Buckley, A.; Turner, J. R., Cell Biology of Tight Junction Barrier Regulation and Mucosal Disease. *Csh Perspect Biol* 2018, *10* (1).

62. Rastegar, D. A.; Tabar, M. S.; Alikhani, M.; Parsamatin, P.; Samani, F. S.; Sabbaghian, M.; Gilani, M. A. S.; Ahadi, A. M.; Meybodi, A. M.; Piryaei, A.; Ansari-Pour, N.; Gourabi, H.; Baharvand, H.; Salekdeh, G. H., Isoform-Level Gene Expression Profiles of Human Y Chromosome Azoospermia Factor Genes and Their X Chromosome Paralogs in the Testicular Tissue of Non-Obstructive Azoospermia Patients. *J Proteome Res* 2015, *14* (9), 3595-3605.

63. Zhu, Y. C.; Zheng, M. H.; Song, D. L.; Ye, L.; Wang, X. D., Global comparison of chromosome X genes of pulmonary telocytes with mesenchymal stem cells, fibroblasts, alveolar type II cells, airway epithelial cells, and lymphocytes. *J Transl Med* 2015, *13*.

64. Zhang, X. T.; Zhang, J. R.; Zhao, W.; Dong, X.; Xin, P.; Liu, X.; Li, X. J.; Jing, Z. F.; Zhang, Z.; Kong, C. Z.; Yu, X. Y., Long non-coding RNA LINC02446 suppresses the proliferation and metastasis of bladder cancer cells by binding with EIF3G and regulating the mTOR signalling pathway. *Cancer Gene Ther* 2021, *28* (12), 1376-1389.

65. Savagner, P., Epithelial-Mesenchymal Transitions: From Cell Plasticity to Concept Elasticity. *Curr Top Dev Biol* 2015, *112*, 273-300.

66. Kyuno, D.; Takasawa, A.; Kikuchi, S.; Takemasa, I.; Osanai, M.; Kojima, T., Role of tight junctions in the epithelial-to-mesenchymal transition of cancer cells. *Bba-Biomembranes* 2021, *1863* (3).

67. Hashimoto, I.; Oshima, T., Claudins and Gastric Cancer: An Overview. *Cancers* 2022, *14* (2).

68. Malfertheiner, P.; Camargo, M. C.; El-Omar, E.; Liou, J. M.; Peek, R.; Schulz, C.; Smith, S. I.; Suerbaum, S., Helicobacter pylori infection. *Nat Rev Dis Primers* 2023, *9* (1).

69. de Brito, B. B.; da Silva, F. A. F.; Soares, A. S.; Pereira, V. A.; Santos, M. L. C.; Sampaio, M. M.; Neves, P. H. M.; de Melo, F. F., Pathogenesis and clinical management of gastric infection. *World J Gastroentero* 2019, *25* (37), 5578-5589.

70. Ho, J. C. M.; Leung, C. C., Management of co-existent tuberculosis and lung cancer. *Lung Cancer* 2018, *122*, 83-87.

71. Christopoulos, A.; Saif, M. W.; Sarris, E. G.; Syrigos, K. N., Epidemiology of active tuberculosis in lung cancer patients: a systematic review. *Clin Respir J* 2014, *8* (4), 375-381.

72. Nalbandian, A.; Yan, B. S.; Pichugin, A.; Bronson, R. T.; Kramnik, I., Lung carcinogenesis induced by chronic tuberculosis infection: the experimental model and genetic control. *Oncogene* 2009, *28* (17), 1928-1938.

73. Holla, S.; Ghorpade, D. S.; Singh, V.; Bansal, K.; Balaji, K. N., BCG promotes tumor cell survival from tumor necrosis factor-α-induced apoptosis. *Molecular Cancer* 2014, *13*.

74. Hwang, S. Y.; Kim, J. Y.; Lee, H. S.; Lee, S.; Kim, D.; Kim, S.; Hyun, J. H.; Shin, J. I.; Lee, K. H.; Han, S. H.; Song, Y. G., Pulmonary Tuberculosis and Risk of Lung Cancer: A Systematic Review and Meta-Analysis. *J Clin Med* 2022, *11* (3).

75. Brabletz, T., To differentiate or not--routes towards metastasis. *Nat Rev Cancer* 2012, *12* (6), 425-36.

76. Gupta, P. K.; Tripathi, D.; Kulkarni, S.; Rajan, M. G. R., H37Rv infected THP-1 cells induce epithelial mesenchymal transition (EMT) in lung adenocarcinoma epithelial cell line (A549). *Cell Immunol* 2016, *300*, 33-40.

77. Leung, C. Y.; Huang, H. L.; Rahman, M. M.; Nomura, S.; Abe, S. K.; Saito, E.; Shibuya, K., Cancer incidence attributable to tuberculosis in 2015: global, regional, and national estimates. *Bmc Cancer* 2020, *20* (1).

78. De La Barrera, S.; Alemán, M.; Musella, R.; Schierloh, P.; Pasquinelli, V.; García, V.; Abbate, E.; Sasiain, M. D., IL-10 down-regulates costimulatory molecules on-pulsed macrophages and impairs the lytic activity of CD4 and CD8 CTL in tuberculosis patients. *Clin Exp Immunol* 2004, *138* (1), 128-138.

79. Chen, X.; Huang, J.; Zhu, H. M.; Guo, Y. P.; Khan, F. A.; Menghwar, H.; Zhao, G.; Guo, A. Z., P27 (MBOV_RS03440) is a novel fibronectin binding adhesin of Mycoplasma bovis. *Int J Med Microbiol* 2018, *308* (7), 848-857.

80. Zhao, G.; Zhu, X. F.; Zhang, H.; Chen, Y. Y.; Schieck, E.; Hu, C. M.; Chen, H. C.; Guo, A., Novel Secreted Protein of MbovP280 Induces Macrophage Apoptosis Through CRYAB. *Frontiers in Immunology* 2021, *12*.

81. Li, T.; He, J.; Cao, H.; Zhang, Y.; Chen, J.; Xiao, Y.; Huang, S. Y., All-atom RNA structure determination from cryo-EM maps. *Nat Biotechnol* 2024.

FIG1

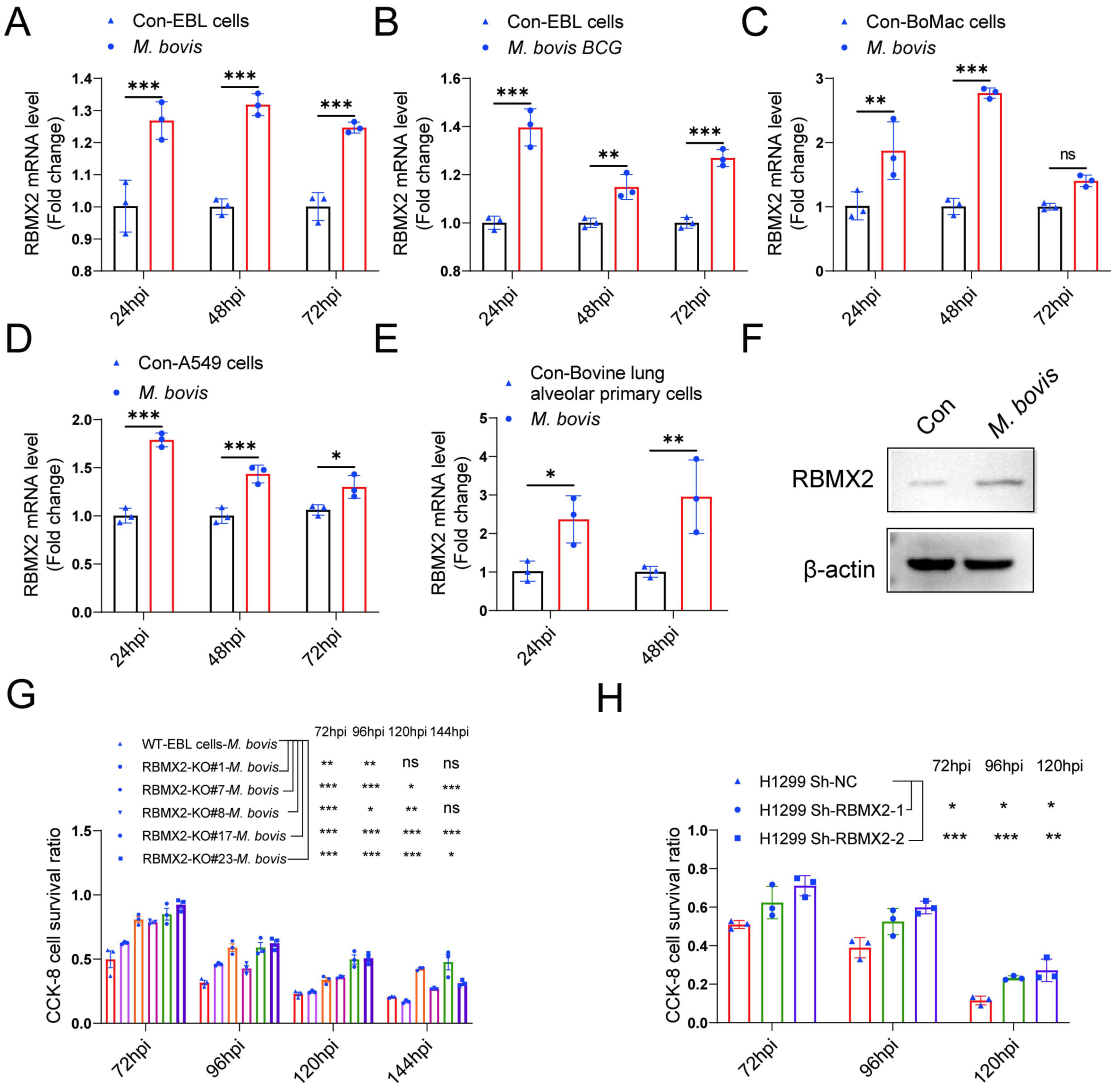

FIGURE 1| Expression of *RBMX2* after infection, and *RBMX2* did not affect cell proliferation but inhibited cell survival during *M. bovis* infection.

(A, B) The expression of *RBMX2* in EBL cells infected by (A) *M. bovis* and (B) *M. bovis* BCG were analyzed by RT-qPCR. Data were represented by fold expression relative to uninfected cells.

(C,-E) The expression of *RBMX2* mRNA in (E) BoMac cells, (F) A549 cells, and (G) bovine lung alveolar primary cells infected by *M. bovis* were analyzed via RT-qPCR. Data were represented by fold expression relative to uninfected cells.

(F) The expression of *RBMX2* in EBL cells infected by *M. bovis was* analyzed by WB. Data were represented by fold expression relative to uninfected cells.

(G) Detection of the ability of different *RBMX2* knockout site Monoclonal EBL cells against *M. bovis* infection by CCK-8 assay. Data were represented by the absorbance value relative to WT EBL cells after *M. bovis* infection.

(H) Detection of the ability of *RBMX2* slicing H1299 cells against *M. bovis* infection by CCK-8 assay. Data were represented by the absorbance value relative to Sh-NC H1299 cells after *M.*

bovis infection.

One-way ANOVA and two-way ANOVA were used to determine the statistical significance of differences between different groups. Ns presents no significance, * presents $p < 0.05$, **presents $p < 0.01$, and *** presents $p < 0.001$ indicate statistically significant differences. Data were representative of at least three independent experiments.

FIG2

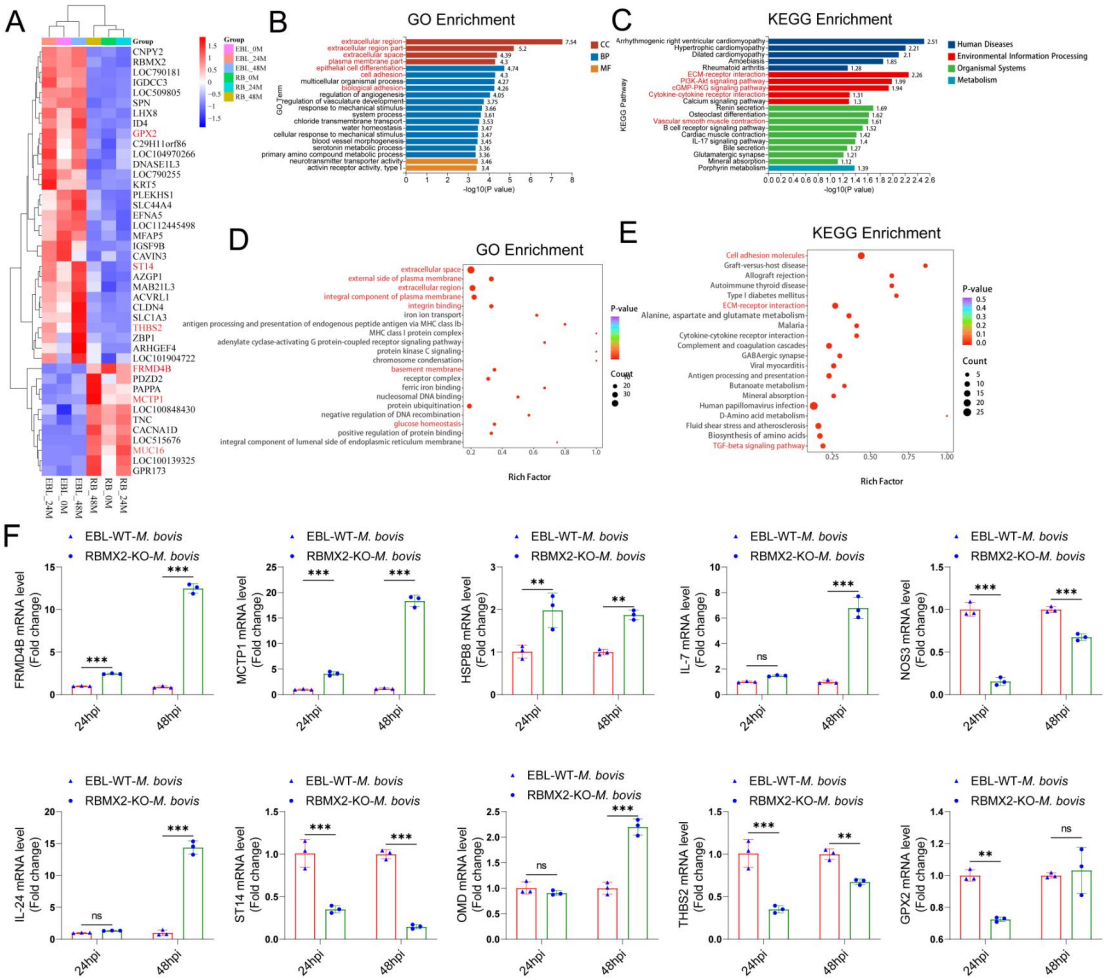

FIGURE 2| Transcriptome and proteomic analysis in *RBMX2* knockout and WT EBL cells after *M. bovis* infection.

(A) The heat map illustrates some genes that had been all enriched in RBMX2 knockout and WT EBL cells after *M. bovis* infection in 0 (2 hpi post-gentamicin, recorded as 0 hpi), 24, and 48hpi. Red represents upregulated genes, and blue represents downregulated genes. Each group represented three independent samples.

(B) GO Analysis of all enriched genes in 0 (2 hpi post-gentamicin, recorded as 0 hpi), 24 and 48hpi. Data were represented as all enriched pathways in RBMX2 knockout EBL cells relative to WT EBL cells after *M. bovis* infection thrice.

(C) KEGG Analysis of all enriched genes in 0 (2 hpi post-gentamicin, recorded as 0 hpi), 24, and 48hpi. Data were represented as all enriched pathways in RBMX2 knockout EBL cells relative to WT EBL cells after *M. bovis* infection in three times.

(D) GO Analysis of all enriched proteins in 48hpi. Data were represented as all enriched pathways in RBMX2 knockout EBL cells relative to WT EBL cells after *M. bovis* infection.

(E) KEGG Analysis of all enriched genes in 48hpi. Data were represented as all enriched pathways in RBMX2 knockout EBL cells relative to WT EBL cells after *M. bovis*-infection (MOI 20) in three times.

(F) Identification the expression of related genes mRNA enriched by RT-qPCR. Data were represented as the fold expression in RBMX2 knockout EBL cells relative to WT EBL cells after *M. bovis* infection.

Two-way ANOVA was used to determine the statistical significance of differences between different groups. Ns presents no significance, * presents $p < 0.05$, **presents $p < 0.01$, and *** presents $p < 0.001$ indicate statistically significant differences.

FIG3

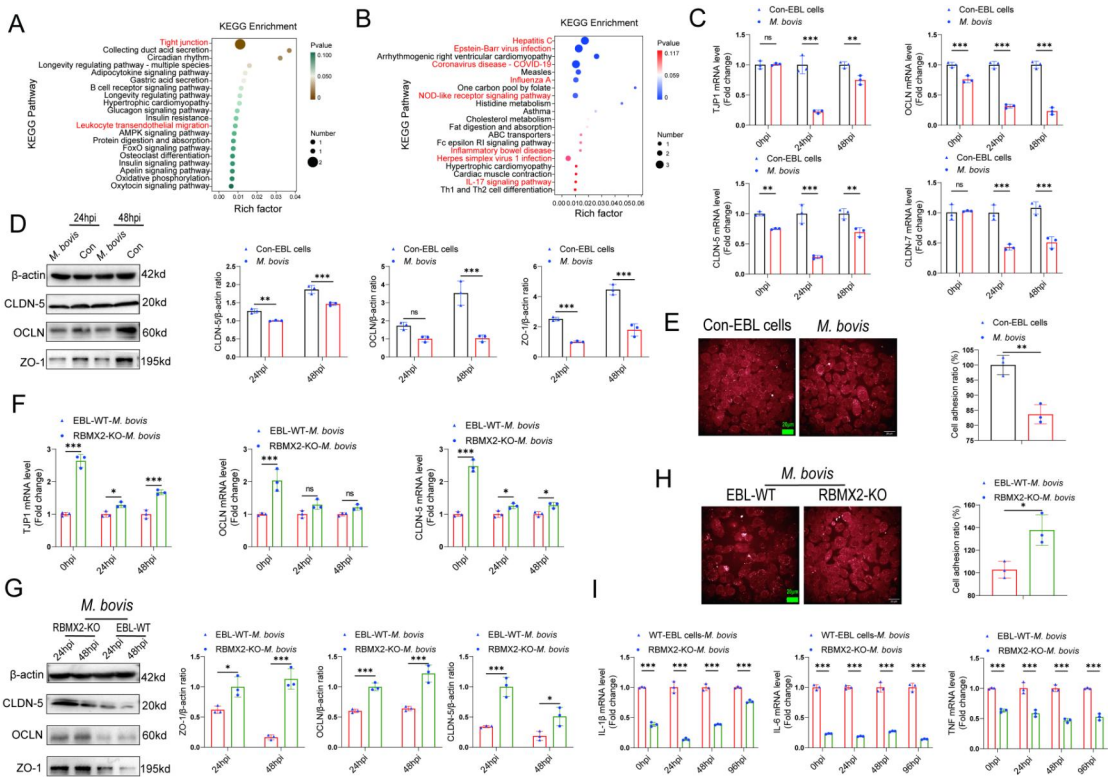

FIGURE 3| *RBMX2* had the potential to induce the disruption of tight junctions in EBL cells after *M. bovis* infection.

(A, B) KEGG analysis was conducted to identify the (A) down-regulated and (B) up-regulated pathways among the enriched genes after *M. bovis* infection of WT EBL cells. Data were relative to WT EBL cells without *M. bovis* infection.

(C, D) The expression of epithelial cells tight junction-related (C) mRNAs (*TJP1*, *CLDN-5*, *CLDN-7,* and *OCLN*) and (D) proteins (ZO-1, CLDN-5, and OCLN) were assessed after *M. bovis* infection of WT EBL cells via RT-qPCR and WB. Data were relative to WT EBL cells without *M. bovis* infection.

(E) Cell adhesion ratio was evaluated via cell adhesion assay after WT EBL cells were infected with *M. bovis* using High-content imaging. Data were relative to WT EBL cells without *M. bovis* infection. Scale bar: 20 μm.

(F, G) The expression of epithelial tight junction-related (F) mRNAs (*TJP1*, *CLDN-5*, and *OCLN*) and (G) proteins (ZO-1, CLDN-5, and OCLN) in *RBMX2* knockout EBL cells after *M. bovis*-infection through RT-qPCR and WB. Data were relative to WT EBL cells with *M. bovis* infection.

(H) Cell adhesion assay was conducted to assess the cell adhesion ratio of *RBMX2* knockout EBL cells after infection with *M. bovis*. Data were relative to WT EBL cells with *M. bovis* infection. Scale bar: 20 μm.

(I) Expression of inflammatory factors-related factors (*IL-6*, *IL-1β*, and *TNF*) were assessed after *RBMX2* knockout EBL cells infected by *M. bovis*. Data were relative to WT EBL cells with *M. bovis* infection.

T-test and Two-way ANOVA were used to determine the statistical significance of differences between different groups. Ns presents no significance, * presents $p < 0.05$, **presents $p < 0.01$, and *** presents $p < 0.001$ indicate statistically significant differences. Data were representative of at least three independent experiments.

FIG4

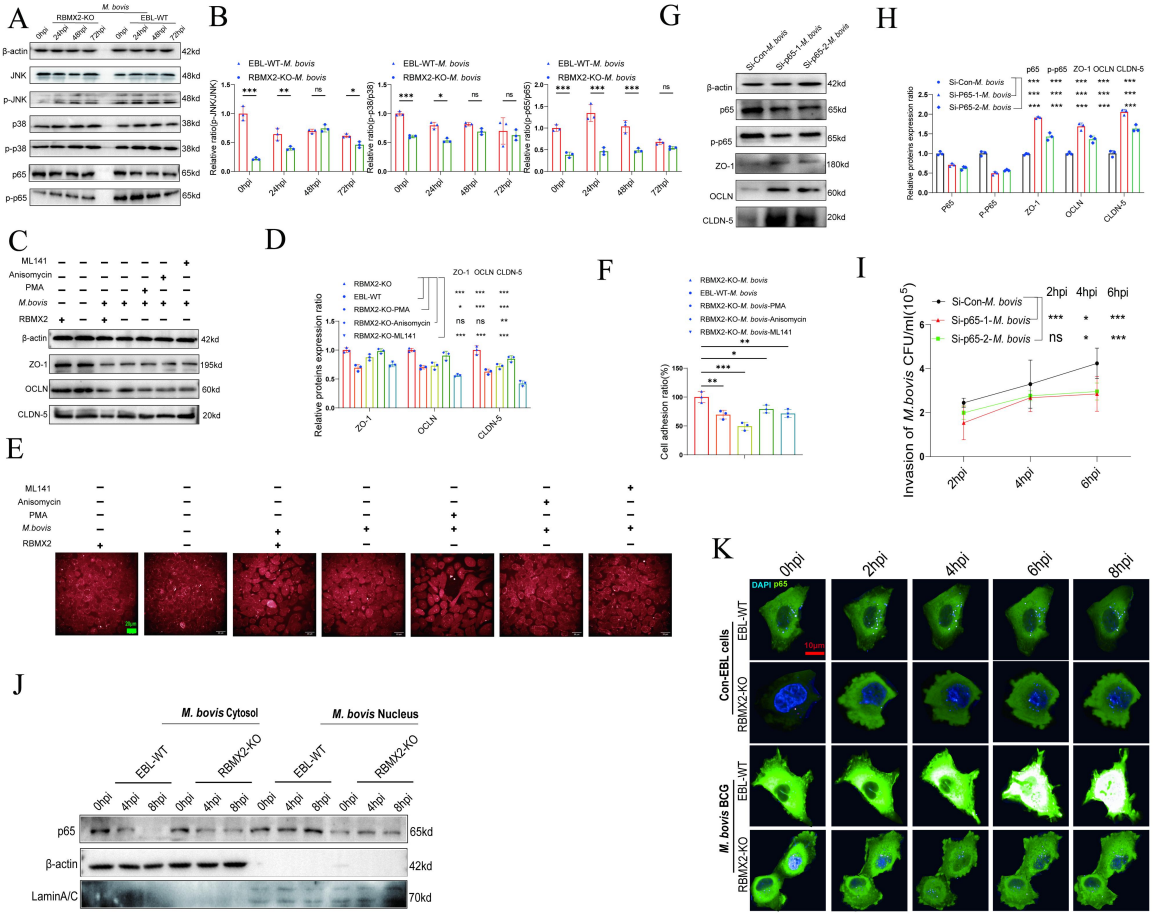

FIGURE 4| *RBMX2* facilitated the disruption of epithelial tight junctions through the promotion of p65 protein phosphorylation and translocation and then enhanced the processes of *M. bovis* adhesion, invasion, and intracellular survival.

(A, B) Activation of the MAPK pathway-related protein and p65 protein were activated after *RBMX2* knockout and WT EBL cells infected by *M. bovis* via WB. Data were relative to WT EBL cells with *M. bovis* infection.

(C, D) Expression of tight junction-related proteins (ZO-1, CLDN-5, and OCLN) was assessed in *RBMX2* knockout EBL cells treated with three p38/p65/JNK pathways activators after *M. bovis* infection via WB. Data were relative to *RBMX2* knockout EBL cells untreated activators with *M. bovis* infection.

(E, F) Evaluate the impact of three *p38/p65/JNK* pathways activators on the ratio of intercellular adhesion via cell adhesion assay. Data were relative to *RBMX2* knockout EBL cells untreated activators with *M. bovis* infection. Scale bar: 20 μm.

(G, H) Evaluate the silencing efficiency of siRNA on p65 protein expression and its impact on the expression of ZO-1, CLDN-5, and OCLN proteins through WB. Data were relative to SiRNA-NC in WT EBL cells with *M. bovis* infection.

(I) The effect of p65 silencing on the invasive ability of *M. bovis* in WT EBL cells. Data were relative to SiRNA-NC in WT EBL cells with *M. bovis* infection.

(J) The effect of *RBMX2* on the nuclear translocation of p65 protein after *M. bovis* infection using WB. β-actin presents cytosol and Lamin A/C presents nucleus. Data were relative to RBMX2 knockout EBL cells after *M. bovis* infection.

(K) The effect of *RBMX2* on the nuclear translocation of p65 protein after *BCG*-infection using High-content real-time imaging. Using pCMV-EGFP-p65 plasmid transfect RBMX2 knockout and WT EBL cells. The nucleus is stained with blue fluorescence. Data were relative to WT EBL cells without BCG infection.

One-way ANOVA and two-way ANOVA were used to determine the statistical significance of differences between different groups. Ns presents no significance, * presents $p < 0.05$, **presents $p < 0.01$, and *** presents $p < 0.001$ indicate statistically significant differences. Data were representative of at least three independent experiments.

FIG5

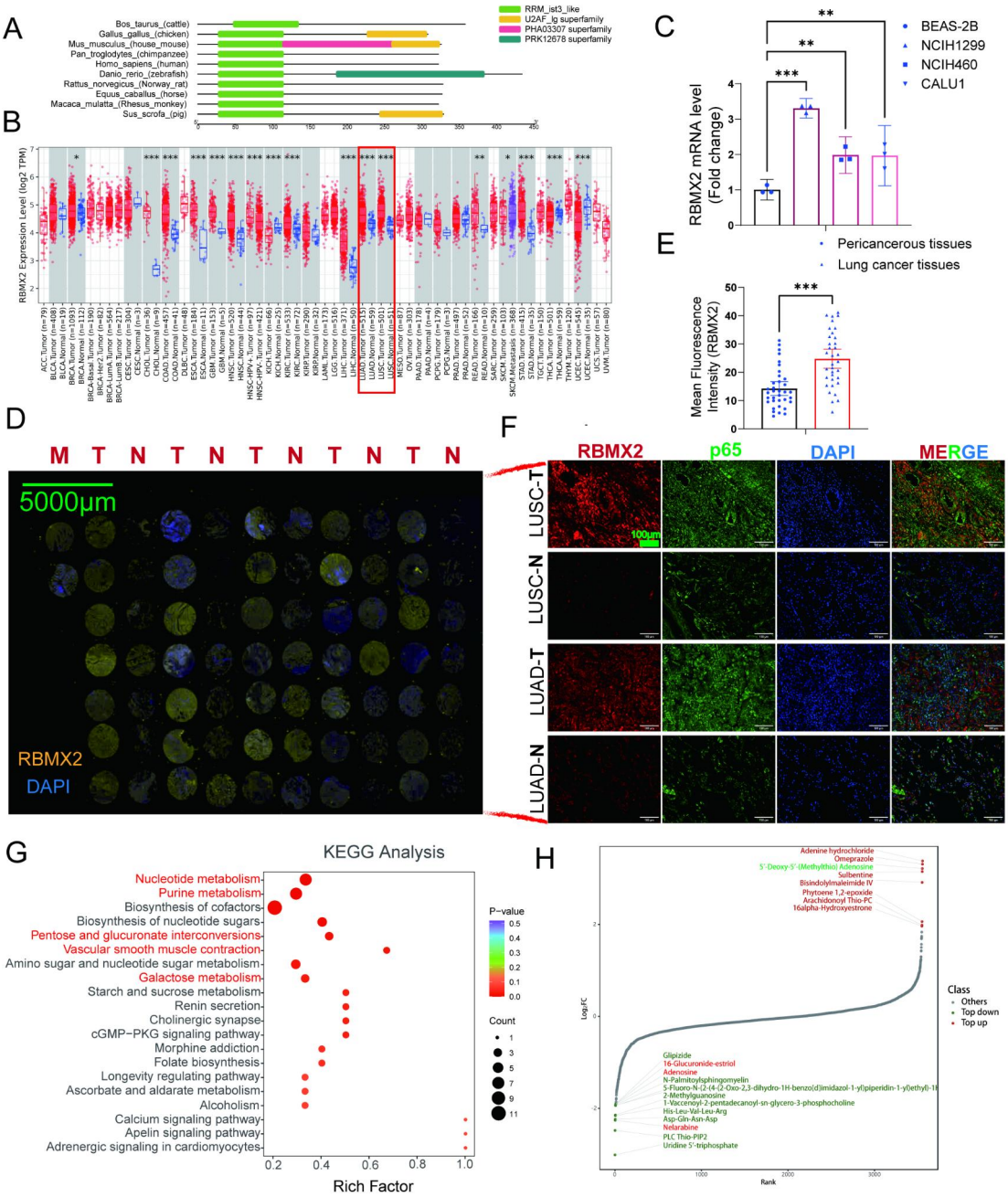

FIGURE 5| *RBMX2* is highly expressed in tumor tissues and regulates cancer-related metabolites

(A) A comparative analysis of the functional domains of the *RBMX2* protein across ten different species.

(B) Analyzing the expression patterns of *RBMX2* in pan cancer using *TIMER2.0* cancer database.

(C) The expression of *RBMX2* in different lung cancer cells and normal lung epithelialcells via RT-qPCR. Data were relative to normal lung epithelialcells (BEAS-2B).

(D-E) The expression of *RBMX2* in lung cancer clinical tissues via IF. RBMX2 is stained with yellow fluorescence, and the nucleus is stained with blue fluorescence. Data were relative to pericancerous lung tissues. Scale Bar: 5000 μm.

(F) The expression of *RBMX2* and p65 in LUAD and LUSC clinical tissues via IF. *RBMX2* is stained with red fluorescence, p65 is stained with green fluorescence, and the nucleus is stained with blue fluorescence. Data were relative to normal lung tissues. Scale Bar: 100 μm.

(G) KEGG analysis of differential metabolite enrichment pathways in *RBMX2* knockout EBL cells compared to WT EBL cells after *M. bovis* infection.

(H) Dynamic distribution map of top 20 differential metabolites in RBMX2 knockout EBL cells compared to WT EBL cells after *M. bovis* infection.

FIG6

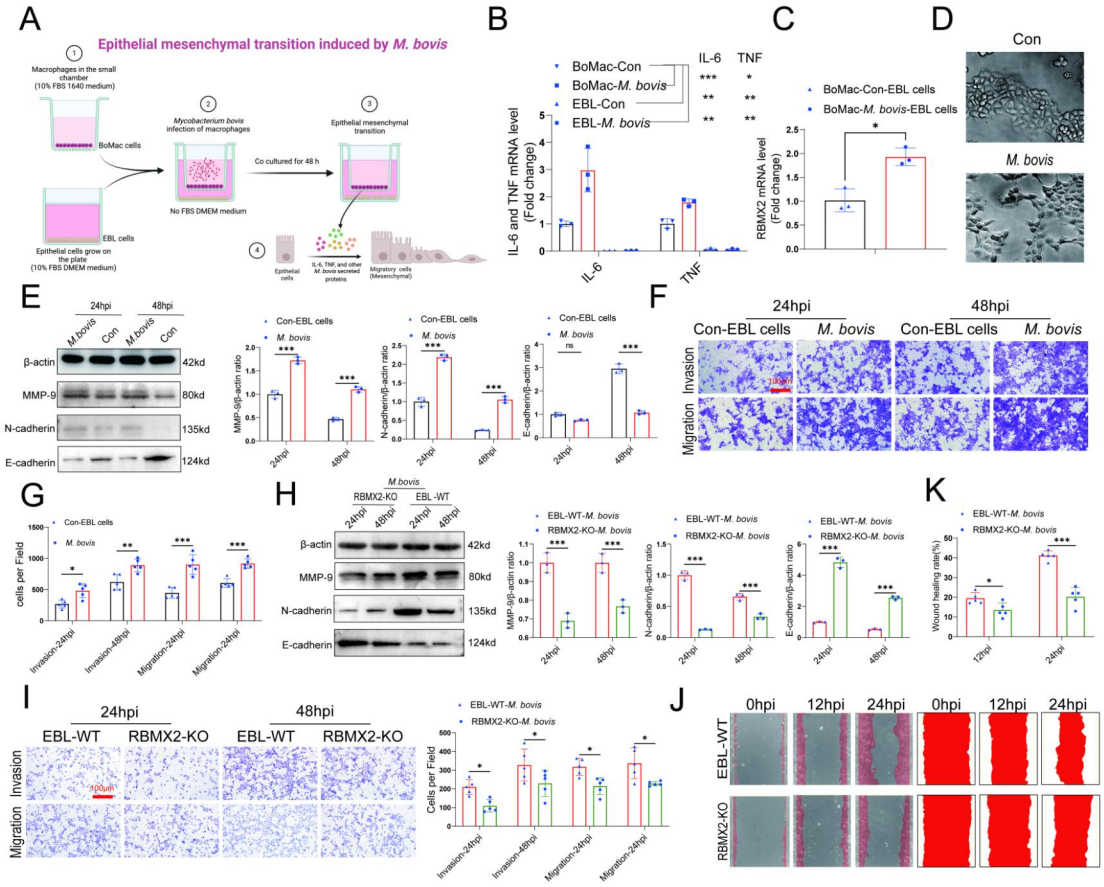

FIGURE 6| *RBMX2* facilitates EMT process in EBL cells after *M. bovis*-infected BoMac cells.

(A) A pattern diagram illustrated a *M. bovis*-infected BoMac cells inducing EMT of EBL cells coculture model, drawing by BioRender.

(B) Detection of IL-6 and TNF expression levels in EBL cells and BoMac cells infected with *M. bovis* using RT-qPCR. Data were relative to BoMac cells without infection of *M. bovis*.

(C) Detection of RBMX2 expression levels in a coculture model EBL cells after *M. bovis* infection using RT-qPCR. Data were relative to BoMac cells without infection of *M. bovis*.

(D) Observation of morphological changes in EBL cells infected with *M. bovis* under electron microscopy.

(E) EMT-related proteins (*MMP-9*, *N-cadherin*, and *E-cadherin*) expression was verified in coculture model EBL cells after *M. bovis* infection through WB. Data were relative to coculture model EBL cells without *M. bovis* infection.

(F, G) The impact of coculture model EBL cells after *M. bovis* infection on migration and invasion

capacity was detected using Transwell assay. Data were relative to coculture model EBL cells without *M. bovis* infection.

(H) The detection of EMT-related proteins (*MMP-9*, *N-cadherin*, and *E-cadherin*) of *RBMX2* knockout EBL cells after *M. bovis-infected* BoMac cells via WB. Data were relative to WT EBL cells after *M. bovis-infected* BoMac cells.

(I) The change in the migratory and invasive capabilities of *RBMX2* knockout EBL cells after *M. bovis-infected* BoMac cells was assessed via Transwell assay. Data were relative to WT EBL cells after *M. bovis-infected* BoMac cells.

(J, K) Validate the changes in migration abilities of *RBMX2* knockout EBL cells after *M. bovis-infected* BoMac cells through wound healing assay. Data were relative to WT EBL cells after *M. bovis-infected* BoMac cells.

T-test and two-way ANOVA were used to determine the statistical significance of differences between different groups. Ns presents no significance, * presents $p < 0.05$, **presents $p < 0.01$, and *** presents $p < 0.001$ indicate statistically significant differences. Data were representative of at least three independent experiments.

FIG7

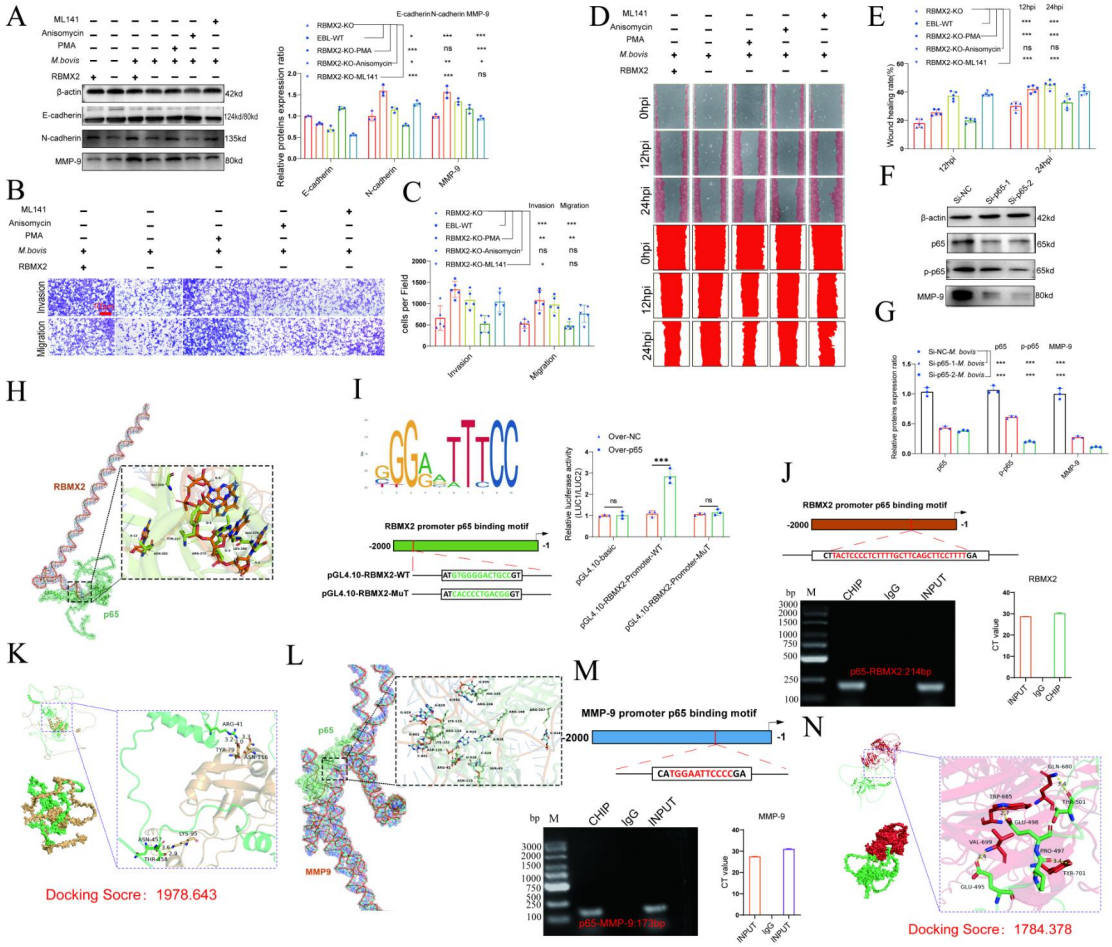

1509 **FIGURE 7| *RBMX2* facilitates the EMT in EBL cells via *p65/MMP-9* pathway.**
1510 (A) Evaluate the impact of pathway activations on expression of EMT-associated proteins (*MMP-9*,
1511 *N-cadherin*, and *E-cadherin*) in *RBMX2* knockout EBL cells after *M. bovis-infected* BoMac cells.
1512 Data were relative to *RBMX2* knockout EBL cells untreated activators.
1513 (B, C) Evaluate the impact of pathway activations on the migratory and invasive capabilities of
1514 RBMX2 knockout EBL cells after *M. bovis-infected* BoMac cells via Transwell assay. Data were
1515 relative to *RBMX2* knockout EBL cells untreated activators.
1516 (D, E) Evaluate the impact of pathway activations on the migratory capabilities of *RBMX2*
1517 knockout EBL cells after *M. bovis-infected* BoMac cells via wound healing assay. Data were
1518 relative to *RBMX2* knockout EBL cells untreated activators.
1519 (F, G) The impact of p65 silencing on the expression of *MMP-9* protein in WT EBL cells after *M.*
1520 *bovis* infection was assessed using WB. Data were relative to SiRNA-NC in WT EBL cells with *M.*
1521 *bovis* infection.
1522 (H) Predicting the binding ability of RBMX2 promoter and p65 using molecular docking dynamics
1523 (I) Verification of *RBMX2* promoter region and p65 interaction using dual luciferase reporter
1524 system.
1525 (I) Using p65 antibody to precipitate p65 protein in EBL cells, and verification of *RBMX2*
1526 promoter region and p65 interaction using Chip-PCR assay.
1527 (K) Predicting potential binding sites for p65 and *RBMX2* via protein docking.
1528 (L) Verification of MMP-9 promoter region and p65 interaction using dual luciferase reporter
1529 system.
1530 (M) Verification of MMP-9 promoter region and p65 interaction using Chip-PCR.
1531 (N) Predicting potential binding sites for p65 and *MMP-9* via protein docking.
1532 Two-way ANOVA was used to determine the statistical significance of differences between
1533 different groups. *$p < 0.05$, **$p < 0.01$, and ***$p < 0.001$ indicate statistically significant
1534 differences. Data were representative of at least three independent experiments.
1535
1536
1537
1538
1539
1540
1541
1542
1543
1544
1545
1546
1547
1548
1549
1550
1551

S1

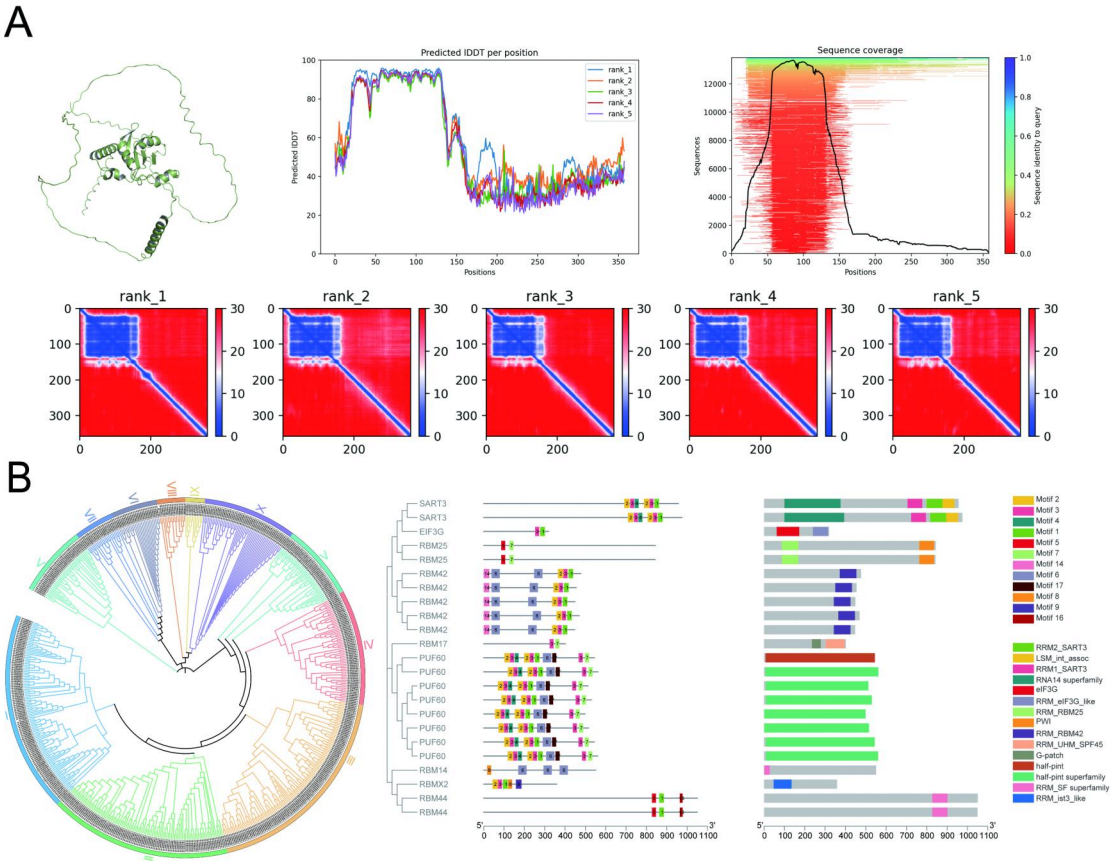

Supplementary Fig 1| Protein structure analysis, subfamily localization.

(A) AlphaFold Multimer predicted the sequence and structure of *RBMX2* protein.

(B) Construction of RBM Gene Family Tree and structural Analysis of genes in *RBMX2* subfamily.

S2

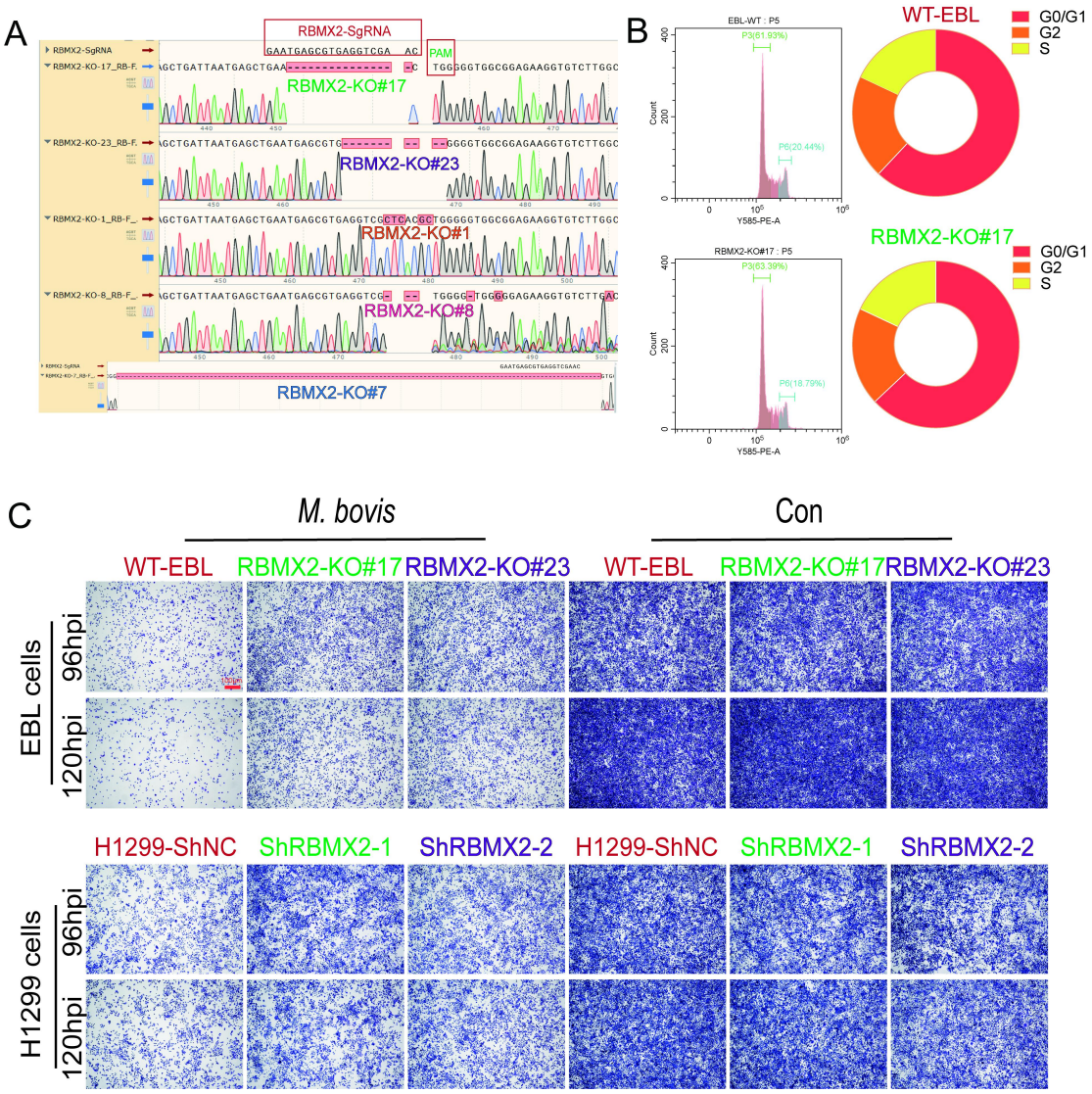

Supplementary Fig 2| The influence of *RBMX2* in cell cycle, cell morphology, cell proliferation, and resistance to *M. bovis* infection.

(A) The different knockout sites of *RBMX2* EBL cells were observed by sequencing compared to the bovine *RBMX2* sequence or WT EBL cells.

(B) Observation of the effect of *RBMX2* knockout on cell cycle of EBL cells by flow cytometry assay. Data are represented as the G0/G1 and S phase relative to WT EBL cells.

(C) The change in cell number of *RBMX2* knockout and silence following 96 and 120 hours of *M. bovis* infection was observed via crystal violet assay in EBL cells and H1299 cells, respectively. Data were represented as the cell number relative to WT EBL cells and H1299-ShNC cells after *M. bovis*-infection. Data were representative of at least three independent experiments.

S3

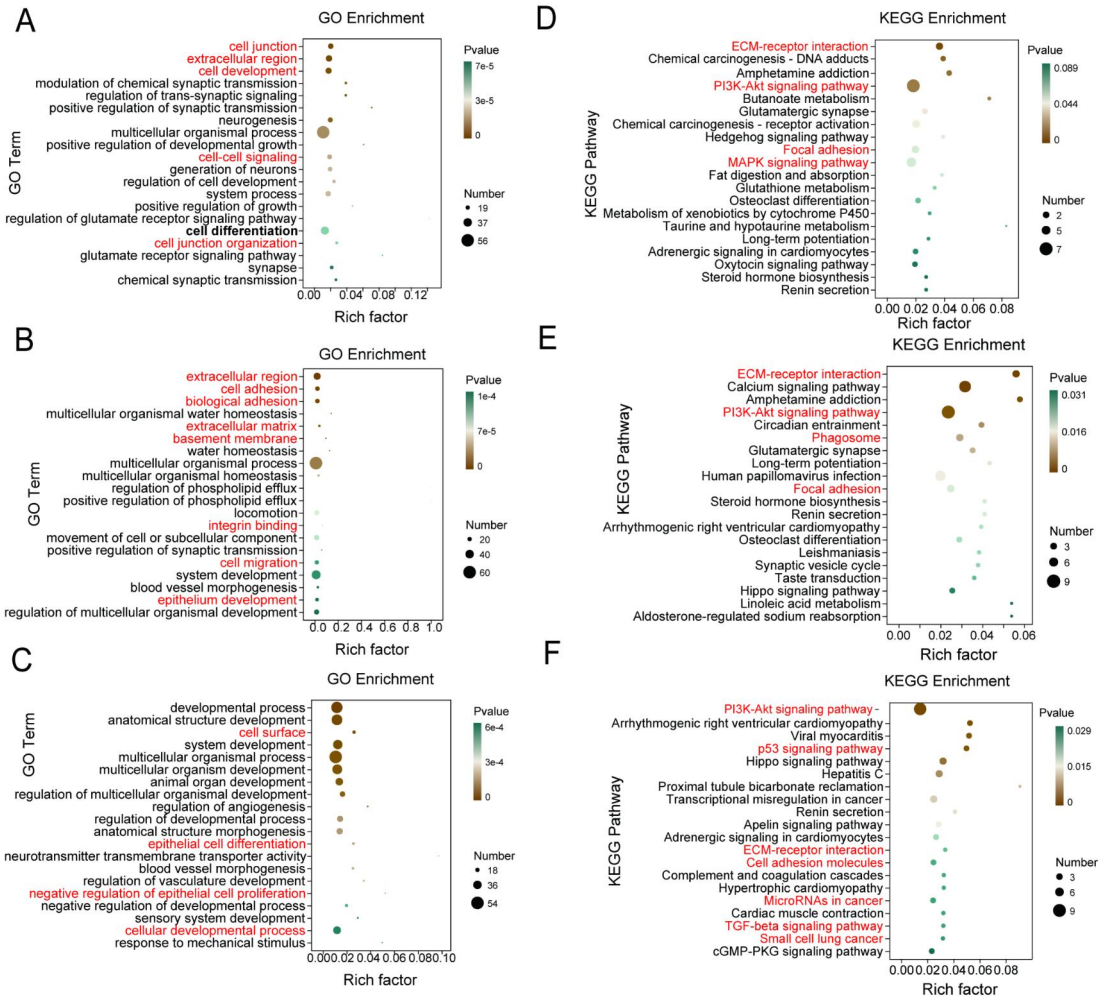

Supplementary Fig 3| Transcriptome analysis in *RBMX2* knockout and WT EBL cells after *M. bovis* infection in different time points.

(A-C) GO analysis of enriched genes of (A) 0 , (B) 24 and (C) 48h after *M. bovis* infection, respectively. Data were in RBMX2 knockout EBL cells relative to WT EBL cells with *M. bovis* infection. The changes of these pathways from cell junction-related pathways in 0 hpi to cell proliferation and differentiation-related pathways in 48 hpi.

(D-F) KEGG analysis of enriched genes of (D) 0, (E) 24 and (F) 48hpi after *M. bovis* infection, respectively. Data were in RBMX2 knockout EBL cells relative to WT EBL cells with *M. bovis* infection. The changes of these pathways from inflammation-related pathways in 0 hpi to cancer-related pathways in 48 hpi.

S4

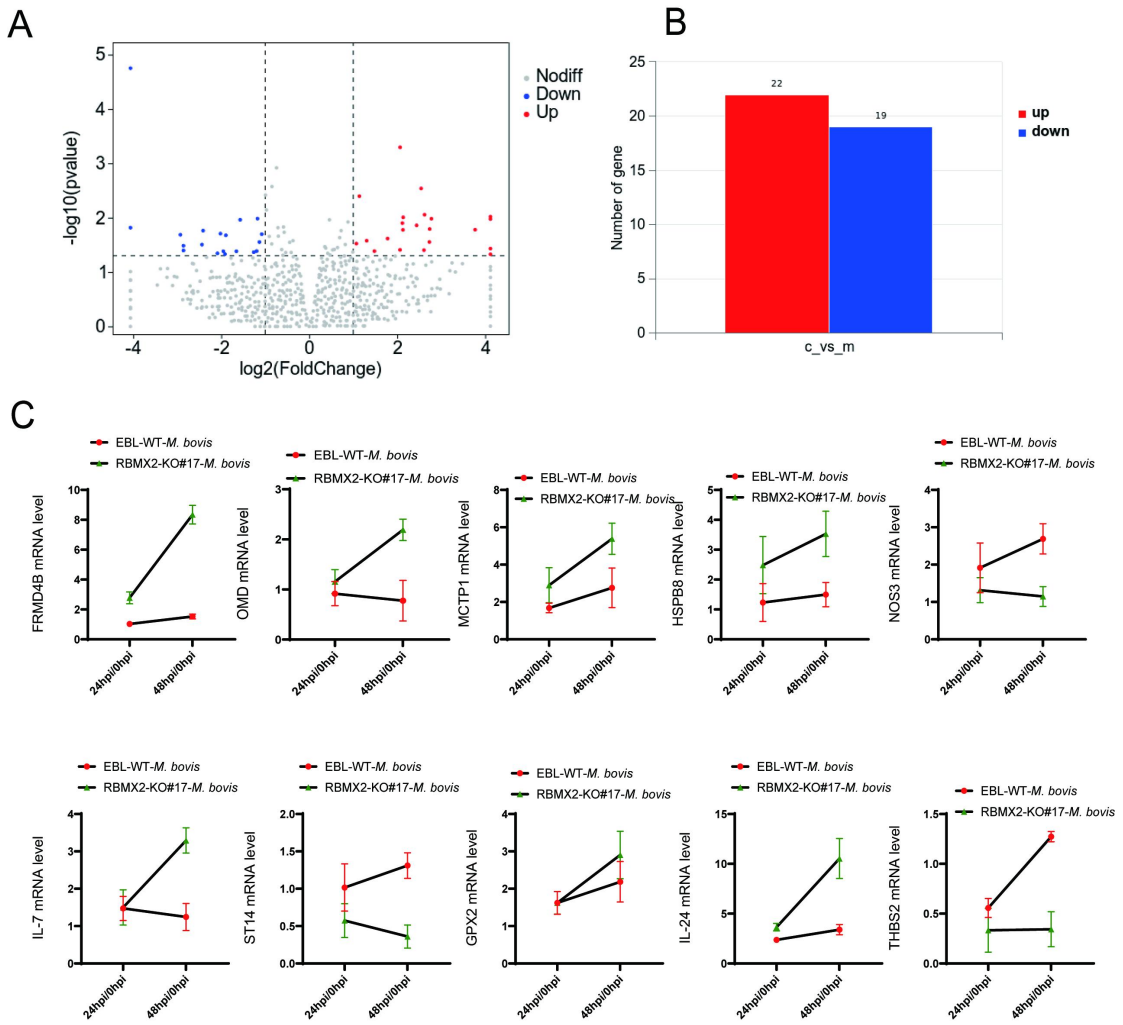

Supplementary Fig 4| Transcriptomic analysis of *M. bovis* infected EBL cells.

(A, B) A volcano map illustrating the transcriptional enrichment genes after WT EBL cells with *M. bovis*-infection. Data were relative to WT EBL cells without *M. bovis* infection.

(C)Identification the expression of related genes mRNA enriched by RT-qPCR. Data were represented as the fold expression in 24hpi/48hpi relative to 0hpi (2 hpi post-gentamicin, recorded as 0 hpi).

S5

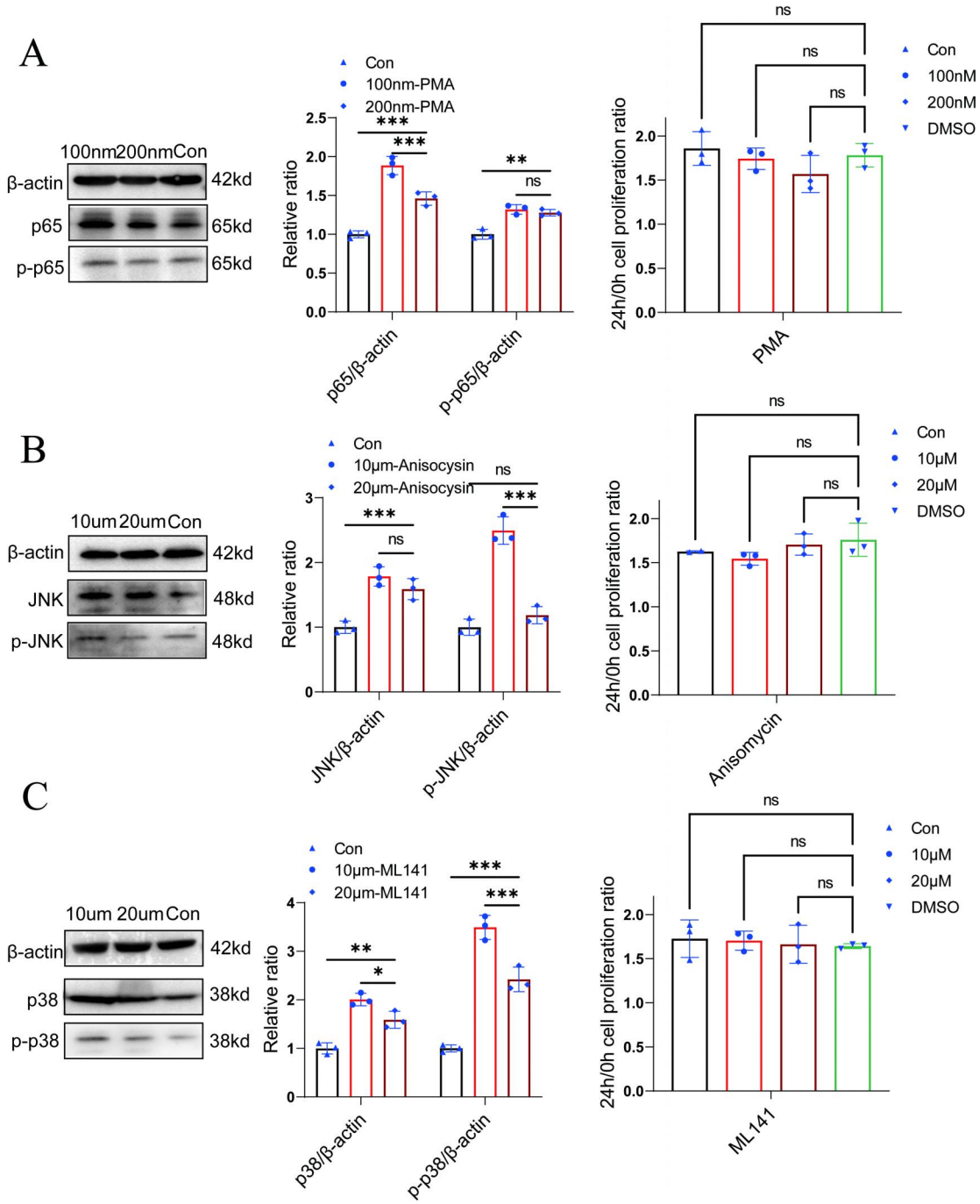

Supplementary Fig 5| The optimal concentration of activators and their impact on cell viability. (A-C) Ascertain the optimal concentration of the three pathway activators and their impact on cellular viability via WB and CCK-8 assays. Data were relative to WT EBL cells untreated activators. One-way ANOVA was used to determine the statistical significance of differences between different groups. Ns presents no significance, **presents $p < 0.01$, and *** presents $p < 0.001$ indicate statistically significant differences.

S6

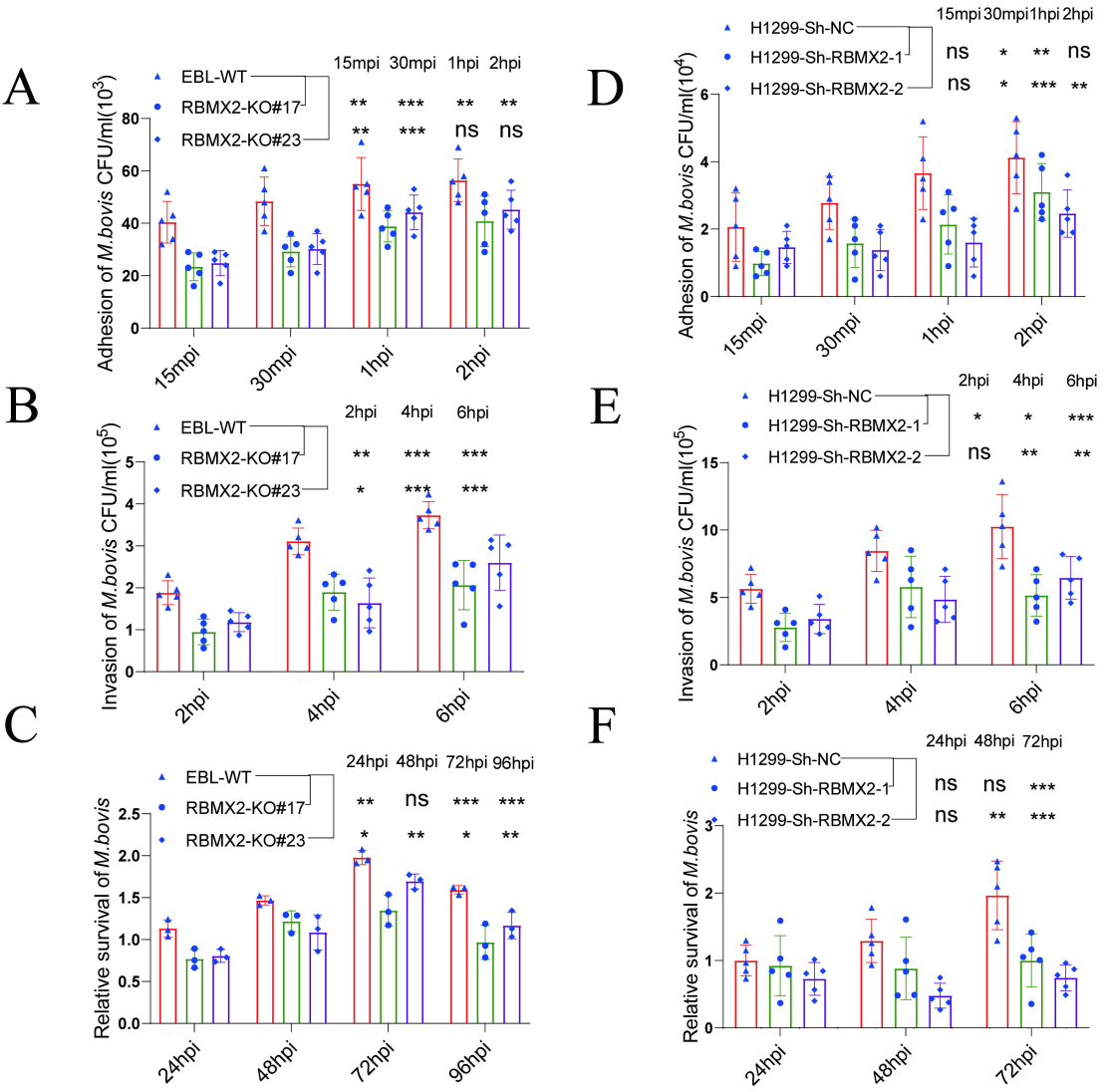

Supplementary Fig 6| *RBMX2* enhanced the processes of *M. bovis* adhesion, invasion, and intracellular survival.

(A, B, C) The impact of *M. bovis* on the adhesion, invasion, and intracellular survival of *RBMX2* knockout and WT EBL cells through plate counting. Data were relative to WT EBL cells after *M. bovis* infection.

(D, E, F) The impact of *M. bovis* on the adhesion, invasion, and intracellular survival of Sh-NC and Sh-RBMX2 H1299 cells through plate counting. Data were relative to H1299 ShNC cells after *M. bovis* infection.

One-way ANOVA and two-way ANOVA were used to determine the statistical significance of differences between different groups. Ns presents no significance, * presents $p < 0.05$, **presents $p < 0.01$, and *** presents $p < 0.001$ indicate statistically significant differences. Data were representative of at least three independent experiments.

S7

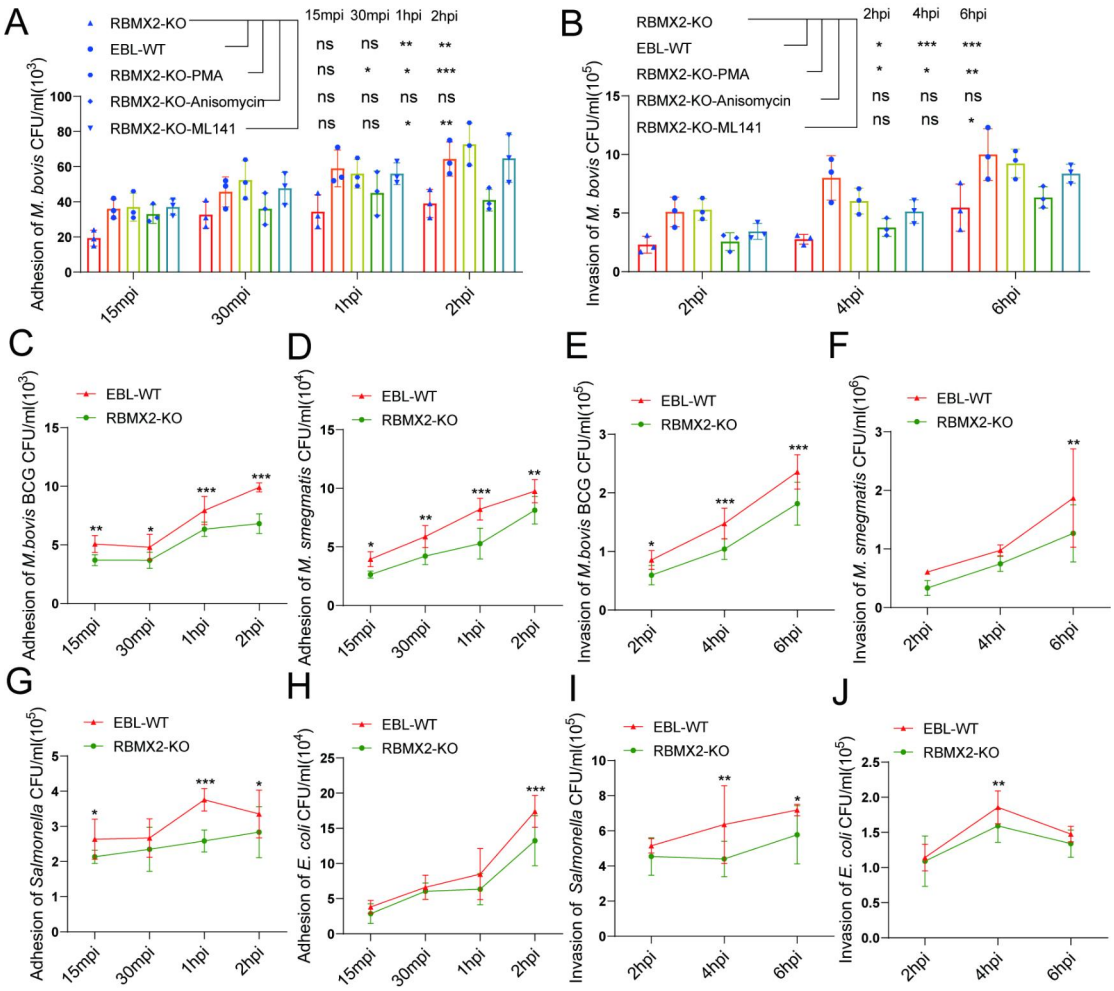

Supplementary Fig 7| *RBMX2* enhanced the processes of pathogen adhesion, invasion, and intracellular survival.

(A, B) The impact of *M. bovis* on the adhesion and invasion of *RBMX2* knockout EBL cells following treatment with related-pathway activators, verified by plate counting. Data were relative to *RBMX2* knockout EBL cells untreated by activators.

(C, D) The impact of *M. bovis* BCG and *M. smegmatis* on the adhesion of *RBMX2* knockout EBL cells through plate counting assay. Data were relative to WT EBL cells after BCG and *M. Smegmatis* infection.

(E, F) The impact of *M. bovis* BCG and *M. smegmatis* on the invasion of *RBMX2* knockout EBL cells through plate counting assay. Data were relative to WT EBL cells after BCG and *M. Smegmatis* infection.

(G, H) The impact of *Salmonella* and *E. coli*, on the adhesion of *RBMX2* knockout EBL cells through plate counting assay. Data were relative to WT EBL cells after *Salmonella* and *E. coli* infection.

(K, L) The impact of *Salmonella* and *E. coli* on the invasion of *RBMX2* knockout EBL cells through plate counting assay. Data were relative to WT EBL cells after *Salmonella* and *E. coli* infection.

One-way and two-way ANOVA were used to determine the statistical significance of differences

between different groups. Ns presents no significance, * presents $p < 0.05$, **presents $p < 0.01$, and *** presents $p < 0.001$ indicate statistically significant differences. Data were representative of at least three independent experiments.

S8

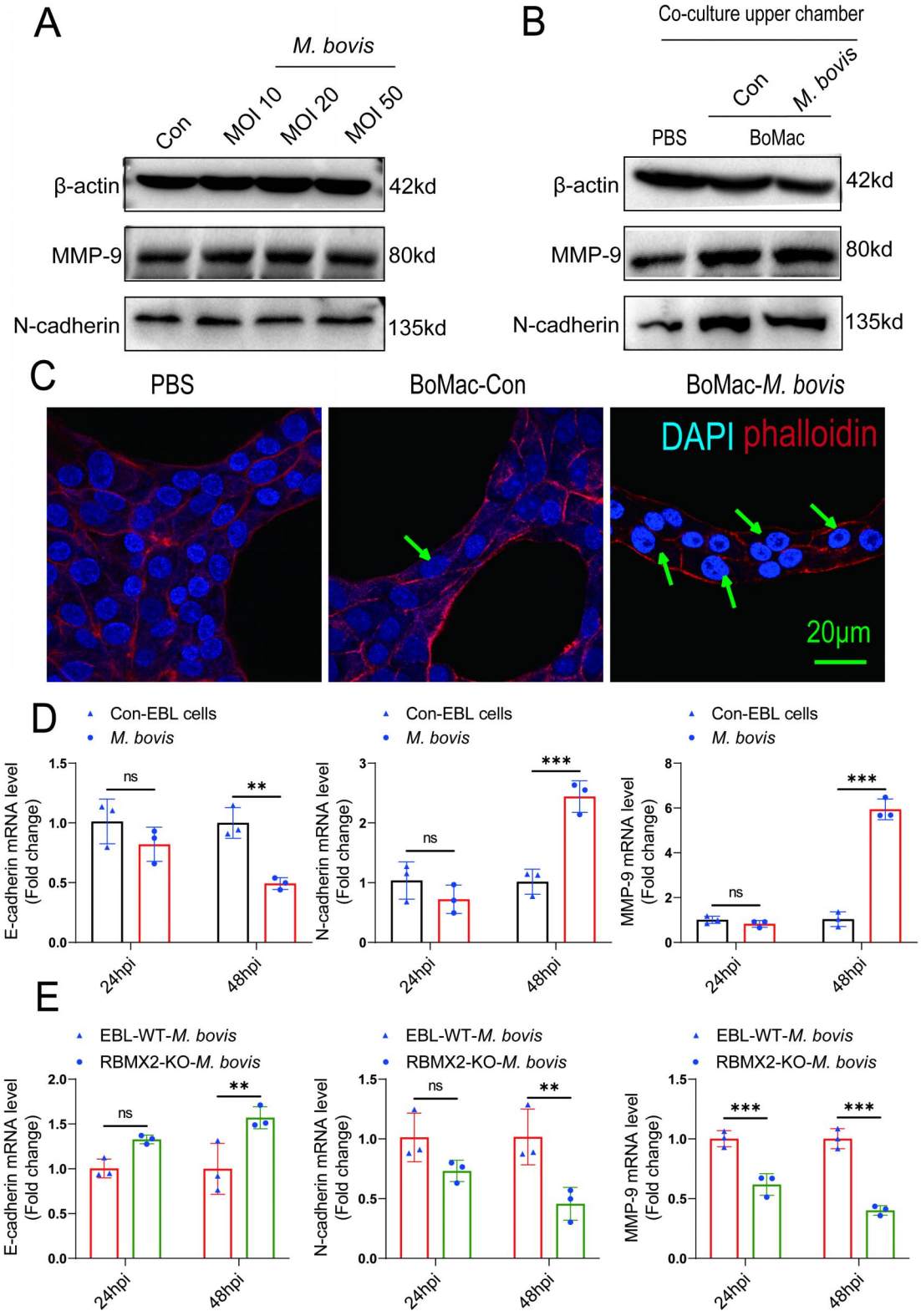

1668 **Supplementary Fig 8| *RBMX2* facilitates EMT process in EBL cells after *M. bovis*-infected BoMac**
1669 **cells.**
1670 (A) WB detection of changes in mesenchymal cell markers (*MMP-9* and *N-cadherin*) after
1671 infection of EBL cells with different infection ratios (10, 20, and 50) of *M. bovis*. Data were relative
1672 to EBL cells without infection of *M. bovis*.
1673 (B) WB detection of the ability of *M. bovis* infection with macrophages (BoMac cells) to induce
1674 epithelial (EBL cells) mesenchymal transition. Data were relative to the addition of PBS in the
1675 upper chamber of the coculture model.
1676 (C) Staining the skeleton of EBL cells in coculture model after *M. bovis* infection using ghost pen
1677 cyclic peptides. The cytoskeleton is labeled with red fluorescence, and the nucleus is stained with
1678 blue fluorescence. Scale Bar: 20 μm.
1679 (D)EMT-related mRNAs (*MMP-9*, *N-cadherin*, and *E-cadherin*) expression was verified in coculture
1680 model EBL cells after *M. bovis* infection through RT-qPCR. Data were relative to coculture model
1681 EBL cells without *M. bovis* infection.
1682 (E) The detection of EMT-related mRNAs (*MMP-9*, *N-cadherin*, and *E-cadherin*) of *RBMX2*
1683 knockout EBL cells after *M. bovis-infected* BoMac cells via RT-qPCR. Data were relative to WT EBL
1684 cells after *M. bovis-infected* BoMac cells.
1685 Two-way ANOVA was used to determine the statistical significance of differences between
1686 different groups. Ns presents no significance, **presents $p < 0.01$, and *** presents $p < 0.001$
1687 indicate statistically significant differences. Data were representative of at least three
1688 independent experiments.
1689
1690
1691
1692
1693
1694
1695
1696
1697
1698
1699
1700
1701
1702
1703

S9

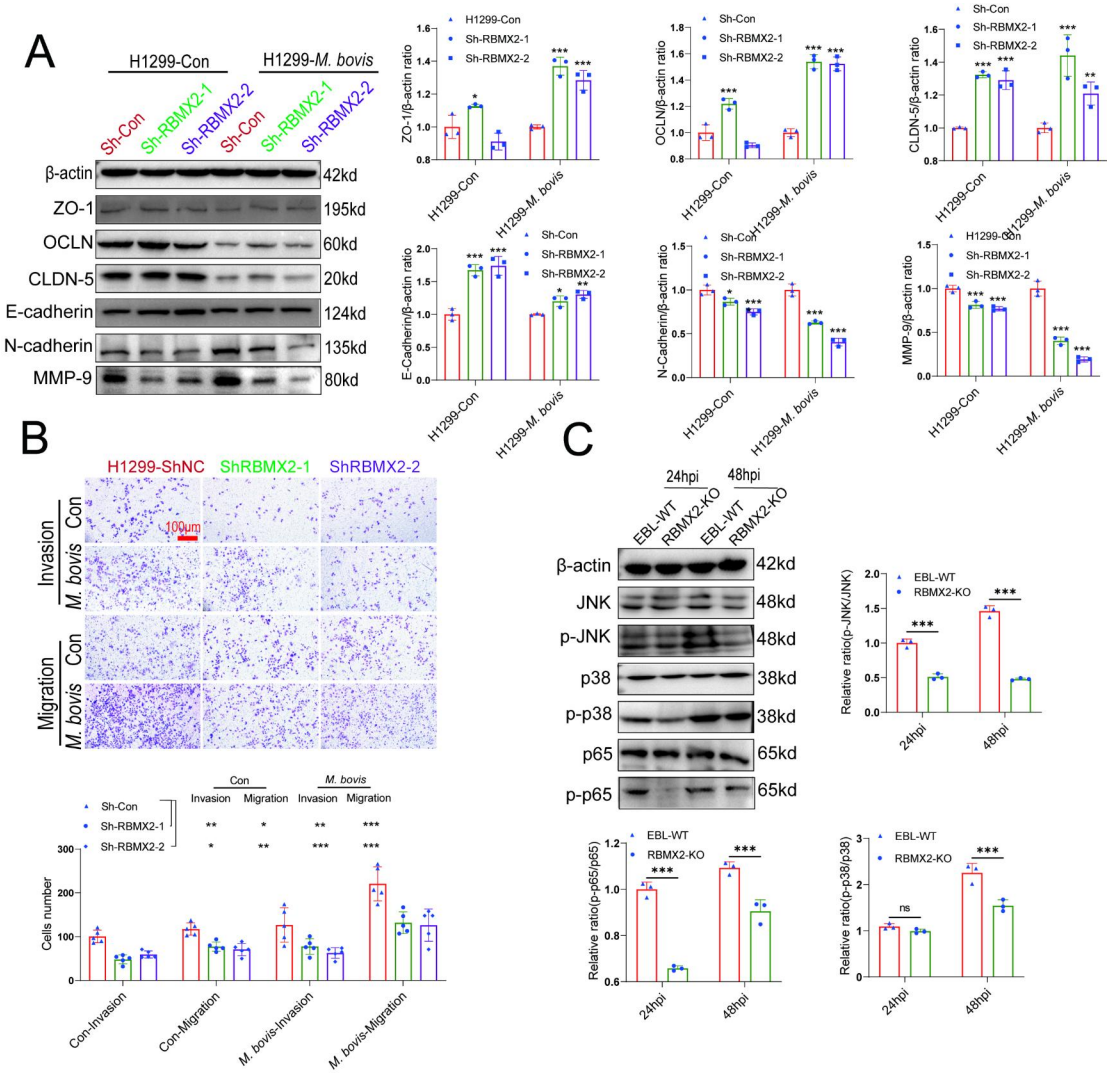

Supplementary Fig 9| *RBMX2* facilitates EMT in H1299 cells.

(A) EMT-related proteins expression was verified in H1299 cells after *M. bovis* infection through WB. Data were relative to H1299 Sh-Con cells.

(B) The change in the migratory and invasive capabilities of H1299 cells was assessed via Transwell assay. Data were relative to H1299 Sh-Con cells. Scale Bar: 100 μm.

(C) Activation of the MAPK pathway-related protein and p65 protein were activated after *RBMX2* knockout and WT EBL cells infected by *M. bovis* in this coculture model via WB. Data were relative to WT EBL cells with *M. bovis* infection.

Two-way ANOVA was used to determine the statistical significance of differences between different groups. *$p < 0.05$, **$p < 0.01$, and ***$p < 0.001$ indicate statistically significant differences. Data were representative of at least three independent experiments.

S TABLE 1

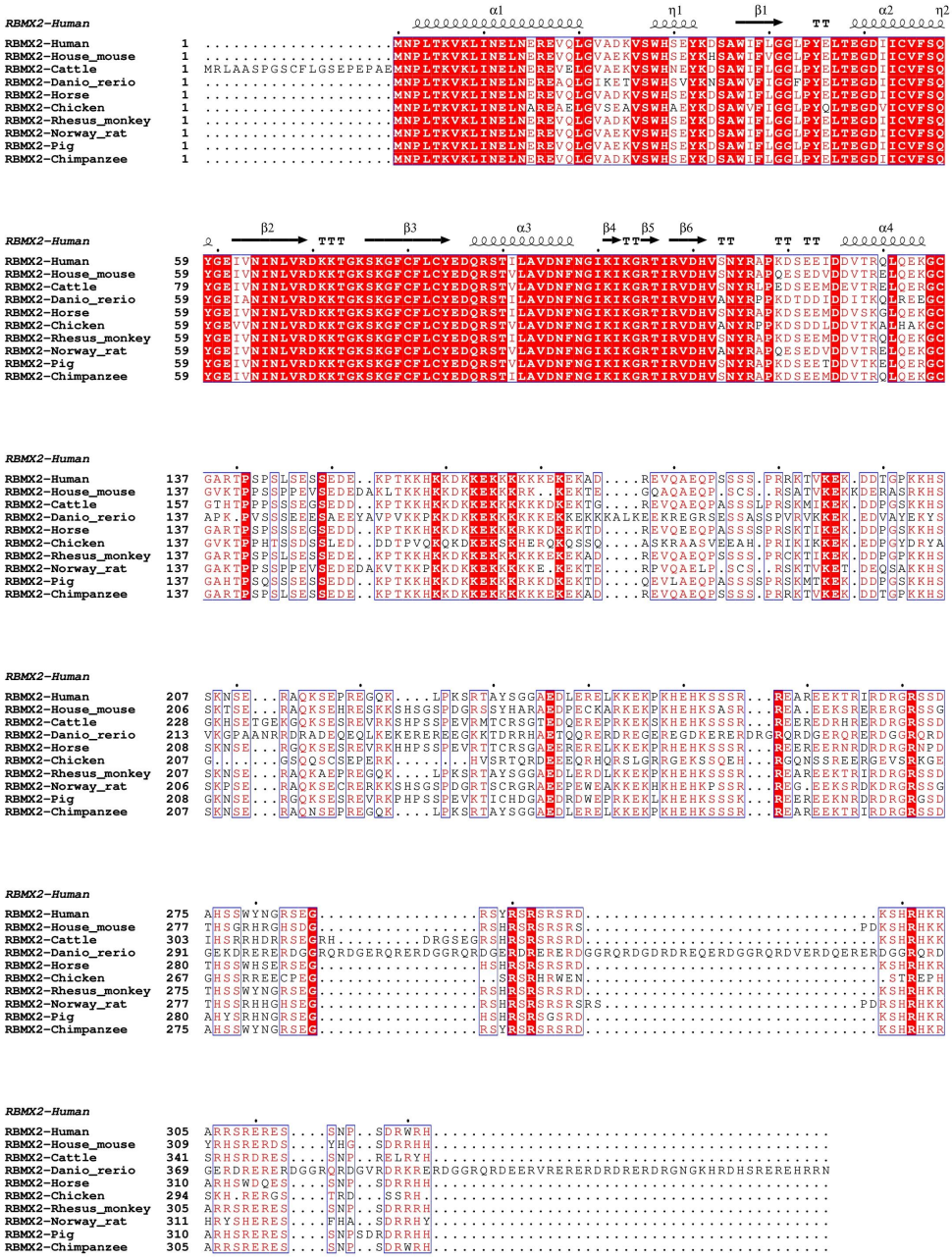

Supplementary Table 1| *RBMX2* exhibits high homology in amino acid sequence alignment across different species